A DIMENSION-REDUCTION BASED COUPLED MODEL OF MESH-REINFORCED SHELLS*

SUNČICA ČANIĆ†, MATEA GALOVIĆ‡, MATKO LJULJ‡, AND JOSIP TAMBAČA‡

Abstract. We formulate a new free-boundary type mathematical model describing the interaction between a shell and a mesh-like structure consisting of thin rods. Composite structures of this type arise in many applications. One example is the interaction between vascular walls treated with vascular devices called stents. The new model embodies two-way coupling between a 2D Naghdi type shell model, and a 1D network model of curved rods, describing no-slip and balance of contact forces and couples (moments) at the contact interface. The work presented here provides a unified framework within which 3D deformation of various composite shell-mesh structures can be studied. In particular, this work provides the first dimension reduction-based fully coupled model of mesh-reinforced shells. Using rigorous mathematical analysis based on variational formulation and energy methods, the existence of a unique weak solution to the coupled shell-mesh model is obtained. The existence result shows that weaker solution spaces than the classical shell spaces can be used to obtain existence, making this model particularly attractive to Finite Element Method-based computational solvers, where Lagrangian elements can be used to simulate the solution. An example of such a solver was developed within Freefem++, and applied to study mechanical properties of four commercially available coronary stents as they interact with vascular wall. The simple implementation, low computational costs, and low memory requirements make this newly proposed model particularly suitable for fast algorithm design and for the coupling with fluid flow in fluid-composite structure interactions problems.

Key words. TO DO

AMS subject classifications. TO DO

1. Introduction. In this paper we formulate a free-boundary type mathematical model of the interaction between shells and mesh-like structures consisting of thin rods. Composite structures of this type arise in many engineering and biological applications where an elastic mesh is used to reinforce the underlying shell structure. The main motivation for this work comes from the study of the interaction between vascular devices called stents, and vascular walls. See Figure 1. Coronary stents have been used to reinforce coronary arteries that suffer from coronary artery disease, which is characterized by occlusion or narrowing of coronary arteries due to plaque deposits. Stents, which are metallic mesh-like tubes, are implanted into coronary arteries to prop the arteries open and to recover normal blood supply to the heart muscle. Understanding the interaction between vascular walls and stents is important in determining which stents produce less complications such as in-stent re-stenosis [7]. Mathematical modeling of stents and other elastic mesh-like structures has been primarily based on using 3D approaches: the entire structure is assumed to be a single 3D structure, and 3D finite elements are used for the numerical approximation of their slender components [3, 13, 14, 18, 22, 23, 24, 25, 34]. It is well known that this approach leads to very poorly conditioned computational problems, and high memory requirements to store the fine computational meshes that are needed to approximate slender bodies with reasonable accuracy. To avoid these difficulties in

*Submitted to the editors DATE.

Funding: The research of Čanić was partially supported by the National Science Foundation under grants DMS-1263572, DMS-1318763, DMS-1311709, and by the Hugh Roy and Lillie Cranz Cullen Distinguished Professorship funds awarded by the University of Houston. J. Tambača was partially supported by HRZZ project grant 9345.

†University of Houston (canic@math.uh.edu, corresponding author)

‡University of Zagreb (matea.galovic@hotmail.com, matko.ljulj@gmail.com, tambaca@math.hr)

modeling mesh-like structures consisting of slender elastic components, Tambača et al. have introduced a 1D network model based on dimension reduction to approximate the slender mesh components using 1D theory of slender rods [32]. The resulting model has been justified both computationally [8] and mathematically [16, 20, 21]. In this model 3D deformation of slender mesh components is approximated using a 1D model of curved rods, and the curved rods are coupled at mesh vertices using two sets of coupling conditions: balance of contact forces and couples, and continuity of displacement and infinitesimal rotation for all the curved rods meeting at the same vertex.

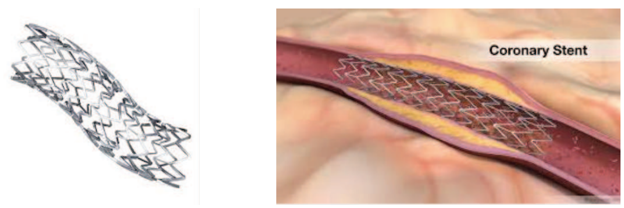

FIG. 1. *Left: Example of an Express-like stent. Right: A stent-reinforced coronary artery.*

In the present manuscript we develop a mathematical framework within which general mesh-like structures modeled by the 1D reduced net/network model discussed above, are coupled to a shell model via two sets of coupling condition: (1) the no-slip condition, and (2) the balance of contact forces and moments, taking place at the contact interface between the shell and mesh. These coupling conditions determine the location of the mesh within the shell, giving rise to a free-boundary type PDE problem.

The shell model that is coupled to the 1D net/network model is a Naghdi-type shell model, recently announced in [31] and analyzed in [33]. This model is chosen because of its several advantages over the classical shell models. Firstly, the model can be entirely formulated in terms of only two unknowns: the displacement $\boldsymbol{u}$ of the middle surface of the shell, and infinitesimal rotation $\boldsymbol{\omega}$ of cross-sections, which are both required to be only in H^1 for the existence of a unique solution to hold. As a consequence, this formulation allows the use of the (less-smooth) Lagrange finite elements for numerical simulation of solutions, which is in contrast with the classical shell models requiring higher regularity. This is a major advantage of this model over the existing shell models. Furthermore, the model is defined in terms of the middle surfaces parameterized by $\boldsymbol{\varphi}$, where $\boldsymbol{\varphi}$ is allowed to be only $W^{1,\infty}$. As a consequence, shells with middle surfaces with corners, or folded plates and shells, are inherently built into the new model. Finally, the model captures the membrane effects, as well as transverse shear and flexural effects, since all three energy terms appear in the total elastic energy of the shell. Although the model is different from the classical membrane shell, or the flexural shell, in each particular regime the solution of the Naghdi type shell model tends to the solution of the corresponding shell model when the thickness of the shell tends to zero [33]. Also, this model can be considered as a small perturbation of the classical Naghdi shell model and that solutions of the model continuously depend on the change in the geometry of the middle surface $\boldsymbol{\varphi}$ in $W^{1,\infty}$. This justifies the use of various approximations of the shell geometry for the purposes of simplifying numerical simulations. Finally, the model can also be seen as a special Cosserat shell model with a single director, see [2], for a particular linear constitutive law. For details see [33]. We note that the shell models that have been considered in modeling vascular walls so far are the classical cylindrical Koiter shell model [9, 5, 6], a reduced Koiter shell model [27], and the membrane model "enhanced with transversal shear" [15].

The Naghdi type shell discussed above, is coupled to the 1D reduced net/network model via a two-way coupling, specified above, describing "glued structures". Using rigorous analysis based on variational formulation and energy estimates, we prove the existence of a unique weak solution to this coupled problem. The solution space provided by this result indicates that only simple Lagrange finite elements can be used for a finite element method-based numerical approximation of the coupled problem. Indeed, to illustrate the use of this model, we developed a finite element method-based solver within the publicly available software Freefem++ [19], and applied it to the stent-vessel coupled problem. Models based on four commercially available stents on the US marked were developed (Palmaz, Xience, Cypher, and Express Stent). The stents were coupled to the mechanics of strait and curved arteries modeled as Naghdi shells. Different responses of the composite stent-vessel configurations to the same pressure loading were recorded and analyzed. Various conclusions related to the performance of each stent inserted in the vessel are deduced. For example, we show that the stiffest stent to bending in the Palmaz-like stent, while the softest is the Xience-like stent. The so called "open cell design" associated with the Xience-like stent, where every other horizontal strut is missing, is associated with higher flexibility (i.e., lower bending rigidity) of Xience-like stents, making this class of stents more appropriate for use in "tortuous", i.e., curved, arteries.

The simple implementation, low computational costs, and low memory requirements make this model particularly attractive for real-time simulations executable on typical laptop computers. Furthermore, the proposed model makes the coupling with a fluid solver computationally feasible, leading to the fluid-composite structure interaction solvers in which the composite structure consisting of a mesh-reinforced shell is resolved in a mathematically accurate and computationally efficient way.

2. The shell model.

We begin by defining our shell model of Naghdi type in arbitrary geometry. Although typical applications in blood flow assume cylindrical geometry, our model can be used to study 2D-1D coupled systems with arbitrary geometry, which we consider here.

2.1. Geometry of the vessel.

The following definition of geometry is classical and can be found in many references, see e.g., [12]. Let $\omega \subset \mathbb{R}^2$ be an open bounded and simply connected set with a Lipschitz-continuous boundary γ. Let $y = (y_\alpha)$ denote a generic point in $\overline{\omega}$ and $\partial_\alpha := \partial/\partial y_\alpha$. Let $\boldsymbol{\varphi} : \overline{\omega} \to \mathbb{R}^3$ be an injective mapping of class C^1 such that the two vectors $\boldsymbol{a}_\alpha(y) = \partial_\alpha \boldsymbol{\varphi}(y)$ are linearly independent at all the points $y \in \overline{\omega}$. They form the covariant basis of the tangent plane to the 2–surface $S = \boldsymbol{\varphi}(\overline{\omega})$ at $\boldsymbol{\varphi}(y)$. The contravariant basis of the same plane is given by the vectors $\boldsymbol{a}^\alpha(y)$ defined by

$$\boldsymbol{a}^\alpha(y) \cdot \boldsymbol{a}_\beta(y) = \delta^\alpha_\beta.$$

We extend these bases to the base of the whole space $\mathbb{R}^3$ by the vector

$$\boldsymbol{a}_3(y) = \boldsymbol{a}^3(y) = \frac{\boldsymbol{a}_1(y) \times \boldsymbol{a}_2(y)}{|\boldsymbol{a}_1(y) \times \boldsymbol{a}_2(y)|}.$$

The first fundamental form or the metric tensor, written in covariant $\mathbf{A}_c = (a_{\alpha\beta})$ or contravariant $\mathbf{A}^c = (a^{\alpha\beta})$ coordinates/components of surface S, are given respectively by

$$a_{\alpha\beta} = \boldsymbol{a}_\alpha \cdot \boldsymbol{a}_\beta, \quad a^{\alpha\beta} = \boldsymbol{a}^\alpha \cdot \boldsymbol{a}^\beta.$$

The area element along S is $\sqrt{a}dy$, where $a := \det \mathbf{A}_c$.

2.2. The Naghdy type shell model. In this section we formulate the Naghdi type shell model, which was recently introduced in [31] and analyzed in [33]. Let $\gamma_0 \subset \partial\omega$ be of positive length. Define the function space V_N to be the space of all H^1 functions with zero trace on γ_0:

$$V_N(\omega) = H^1_{\gamma_0}(\omega;\mathbb{R}^3) \times H^1_{\gamma_0}(\omega;\mathbb{R}^3) = \left\{(\boldsymbol{v},\boldsymbol{w}) \in H^1(\omega;\mathbb{R}^3)^2 : \boldsymbol{v}|_{\gamma_0} = \boldsymbol{w}|_{\gamma_0} = 0\right\}.$$

This function space is a Hilbert space when equipped with the norm

$$\|(\boldsymbol{v},\boldsymbol{w})\|_{V_N(\omega)} = \left(\|\boldsymbol{v}\|^2_{H^1(\omega;\mathbb{R}^3)} + \|\boldsymbol{w}\|^2_{H^1(\omega;\mathbb{R}^3)}\right)^{1/2}.$$

In the notation $(\boldsymbol{u},\boldsymbol{\omega}) \in V_N(\omega)$, $\boldsymbol{u}$ is the displacement vector of the middle surface of the shell, while $\boldsymbol{\omega}$ is the infinitesimal rotation of the cross–sections. A cross-section is a segment perpendicular to the middle surface in undeformed configuration. To define the weak formulation of our Naghdi type shell, we introduce the following bilinear forms on $V_N(\omega)$:

$$\begin{aligned} B_{ms}((\boldsymbol{u},\boldsymbol{\omega}),(\boldsymbol{v},\boldsymbol{w})) &:= h\int_\omega \mathbf{Q}\mathcal{C}_m(\mathbf{Q}^T \left[\begin{array}{cc} \partial_1\boldsymbol{u} + \boldsymbol{a}_1\times\boldsymbol{\omega} & \partial_2\boldsymbol{u} + \boldsymbol{a}_2\times\boldsymbol{\omega}\end{array}\right]) \\ &\qquad \cdot \left[\begin{array}{cc} \partial_1\boldsymbol{v} + \boldsymbol{a}_1\times\boldsymbol{w} & \partial_2\boldsymbol{v} + \boldsymbol{a}_2\times\boldsymbol{w}\end{array}\right]\sqrt{a}dx, \\ B_f((\boldsymbol{u},\boldsymbol{\omega}),(\boldsymbol{v},\boldsymbol{w})) &:= \frac{h^3}{12}\int_\omega \mathbf{Q}\mathcal{C}_f(\mathbf{Q}^T\nabla\boldsymbol{\omega})\cdot\nabla\boldsymbol{w}\sqrt{a}dx, \\ a_{\text{shell}}((\boldsymbol{u},\boldsymbol{\omega}),(\boldsymbol{v},\boldsymbol{w})) &:= B_{ms}((\boldsymbol{u},\boldsymbol{\omega}),(\boldsymbol{v},\boldsymbol{w})) + B_f((\boldsymbol{u},\boldsymbol{\omega}),(\boldsymbol{v},\boldsymbol{w})). \end{aligned} \tag{2.1}$$

The shell model we consider in this paper is given by: find $(\boldsymbol{u},\boldsymbol{\omega}) \in V_N(\omega)$ such that

$$a_{\text{shell}}((\boldsymbol{u},\boldsymbol{\omega}),(\boldsymbol{v},\boldsymbol{w})) = \int_\omega \boldsymbol{f}\cdot\boldsymbol{v}\sqrt{a}dx, \qquad (\boldsymbol{v},\boldsymbol{w}) \in V_N(\omega). \tag{2.2}$$

The term $B_{ms}((\boldsymbol{u},\boldsymbol{\omega}),(\boldsymbol{u},\boldsymbol{\omega}))$ describes the extensibility and shearability of the shell as it measures the membrane and shear energy. The term $B_f((\boldsymbol{u},\boldsymbol{\omega}),(\boldsymbol{u},\boldsymbol{\omega}))$ on $V_F(\omega)$ measures the flexural energy. The shell thickness is denoted by h, $\boldsymbol{f}$ is the surface force density, while the elasticity tensors $\mathcal{C}_m$, $\mathcal{C}_f : M_{3,2}(\mathbb{R}) \to M_{3,2}(\mathbb{R})$ are given by

$$\begin{aligned} \mathcal{C}_m\hat{\mathbf{C}}\cdot\hat{\mathbf{D}} &= \frac{2\lambda\mu}{\lambda+2\mu}(\mathbf{I}\cdot\mathbf{C})(\mathbf{I}\cdot\mathbf{D}) + 2\mu\mathbf{A}_c\mathbf{C}\mathbf{A}^c\cdot\mathbf{D} + \mu\mathbf{A}^c\boldsymbol{c}\cdot\boldsymbol{d}, \\ \mathcal{C}_f\hat{\mathbf{C}}\cdot\hat{\mathbf{D}} &= a\mathcal{A}(\mathbf{J}\mathbf{C})\cdot\mathbf{J}\mathbf{D} + a\mathcal{B}_f\boldsymbol{c}\cdot\boldsymbol{d}, \end{aligned} \tag{2.3}$$

where we have used the notation $\hat{\mathbf{Q}} = \left[\begin{array}{cc}\boldsymbol{a}^1 & \boldsymbol{a}^2\end{array}\right]$, $\mathbf{Q} = \left[\begin{array}{ccc}\boldsymbol{a}^1 & \boldsymbol{a}^2 & \boldsymbol{a}^3\end{array}\right]$ and

$$\hat{\mathbf{C}} = \left[\begin{array}{c}\mathbf{C}\\ \boldsymbol{c}^T\end{array}\right],\ \hat{\mathbf{D}} = \left[\begin{array}{c}\mathbf{D}\\ \boldsymbol{d}^T\end{array}\right] \in M_{3,2}(\mathbb{R}), \quad \mathbf{C},\mathbf{D} \in M_2(\mathbb{R}), \boldsymbol{c},\boldsymbol{d} \in \mathbb{R}^2, \quad \mathbf{J} = \left[\begin{array}{cc} 0 & 1\\ -1 & 0\end{array}\right].$$

The matrix $\mathcal{B}_f \in M_2(\mathbb{R})$ is assumed to be positive definite and the elasticity tensor $\mathcal{A}$ is given by

$$\mathcal{A}\mathbf{D} = \frac{2\lambda\mu}{\lambda+2\mu}(\mathbf{A}^c\cdot\mathbf{D})\mathbf{A}^c + 2\mu\mathbf{A}^c\mathbf{D}\mathbf{A}^c, \qquad \mathbf{D} \in M_2(\mathbb{R}),$$

where λ and μ are the Lamé coefficients. We assume that $3\lambda + 2\mu, \mu > 0$. When applied to symmetric matrices the tensor $\mathcal{A}$ is the same as the elasticity operator that appears in the classical shell theories.

The shell model we use is of Naghdi type since the shell energy contains the membrane, the shear and the flexural energy. This model can be viewed as a small perturbation of the classical Naghdi shell model but with some superior properties.

By considering equation (2.2) on the subspace of $V_N(\omega)$ for which

$$\boldsymbol{w} = \frac{1}{\sqrt{a}}\left((\partial_2\boldsymbol{v}\cdot\boldsymbol{a}_3)\boldsymbol{a}_1 - (\partial_1\boldsymbol{v}\cdot\boldsymbol{a}_3)\boldsymbol{a}_2 + \frac{1}{2}(\partial_1\boldsymbol{v}\cdot\boldsymbol{a}_2 - \partial_2\boldsymbol{v}\cdot\boldsymbol{a}_1)\boldsymbol{a}_3\right) \tag{2.4}$$

one obtains the model of the Koiter shell type discussed in [31], which can be seen as a small perturbation of the classical Koiter shell model. The condition in the function space implies that the shear energy is zero and that the deformed cross–sections remain, within linear theory, perpendicular to the deformed middle surface. Furthermore, the assumption that both, the membrane and shear energy are zero, i.e. $B_{ms}((\boldsymbol{v},\boldsymbol{w}),(\boldsymbol{v},\boldsymbol{w})) = 0$ implies, among other things (2.4), and further reduces the function space. On this function space the model considered in this manuscript is exactly equal to the classical flexural shell model.

If we neglect flexural energy B_f from the elastic energy in the Naghdi type shell model (2.2) the shear energy turns to be zero and we obtain exactly the membrane shell model, as discussed in Lemma 3.3 and Section 3.3 in [33].

The existence of a unique solution for this shell model can be obtained under the classical assumptions that $\boldsymbol{\varphi} \in W^{1,\infty}(\omega;\mathbb{R}^3)$, $3\lambda + 2\mu, \mu > 0$, $\mathcal{B}_f$ is positive definite, and $\mathbf{A}^c, \mathbf{A}_c$ are uniformly positive definite, i.e., the spectrum σ and the area element $\sqrt{a}$ are such that

$$\operatorname*{ess\,inf}_{y\in\omega} \sigma(\mathbf{A}^c(y)), \operatorname*{ess\,inf}_{y\in\omega} \sigma(\mathbf{A}_c(y)), \operatorname*{ess\,inf}_{y\in\omega} a(y) > 0. \tag{2.5}$$

For a smooth geometry, e.g., for $\boldsymbol{\varphi} \in C^1(\overline{\omega};\mathbb{R}^3)$ such that $\partial_1\boldsymbol{\varphi}(y), \partial_2\boldsymbol{\varphi}(y)$ are linearly independent for all $y \in \overline{\omega}$, these conditions hold. Note also that $\mathbf{A}^c = \mathbf{A}_c^{-1}$. Under these assumptions it is easy to show that $\mathcal{C}_m$ and $\mathcal{C}_f$ are positive definite (with constants c_m and c_f, respectively) and that the following inequality holds or all $(\boldsymbol{v},\boldsymbol{w}) \in V_N(\omega)$ [31]:

$$\begin{aligned}
&\|(\boldsymbol{v},\boldsymbol{w})\|_{V_N(\omega)} \\
&\quad\le C_N\left(\|\begin{bmatrix} \partial_1\boldsymbol{v} + \boldsymbol{a}_1\times\boldsymbol{w} & \partial_2\boldsymbol{v} + \boldsymbol{a}_2\times\boldsymbol{w}\end{bmatrix}\|^2_{L^2(\omega;M_{3,2}(\mathbb{R}))} + \|\nabla\boldsymbol{w}\|^2_{L^2(\omega;M_{3,2}(\mathbb{R}))}\right)^{1/2},
\end{aligned}$$

where $C_N > 0$. From here one can easily see that a_{shell} is positive definite on $V_N(\omega)$:

$$\begin{aligned}
a_{\text{shell}}((\boldsymbol{v},\boldsymbol{w}),(\boldsymbol{v},\boldsymbol{w})) &= B_{ms}((\boldsymbol{v},\boldsymbol{w}),(\boldsymbol{v},\boldsymbol{w})) + B_f((\boldsymbol{v},\boldsymbol{w}),(\boldsymbol{v},\boldsymbol{w})) \\
&\ge c_m\|\mathbf{Q}^T\begin{bmatrix} \partial_1\boldsymbol{v} + \boldsymbol{a}_1\times\boldsymbol{w} & \partial_2\boldsymbol{v} + \boldsymbol{a}_2\times\boldsymbol{w}\end{bmatrix}\|^2_{L^2(\omega;M_{3,2}(\mathbb{R}))} \\
&\quad + \frac{1}{12}c_f\|\mathbf{Q}^T\nabla\boldsymbol{w}\|^2_{L^2(\omega;M_{3,2}(\mathbb{R}))} \\
&\ge c\left(\|\begin{bmatrix} \partial_1\boldsymbol{v} + \boldsymbol{a}_1\times\boldsymbol{w} & \partial_2\boldsymbol{v} + \boldsymbol{a}_2\times\boldsymbol{w}\end{bmatrix}\|^2_{L^2(\omega;M_{3,2}(\mathbb{R}))} + \|\nabla\boldsymbol{w}\|^2_{L^2(\omega;M_{3,2}(\mathbb{R}))}\right) \\
&\ge C_{\text{shell}}\|(\boldsymbol{v},\boldsymbol{w})\|^2_{V_N(\omega)}.
\end{aligned} \tag{2.6}$$

Now the existence of a unique solution for the shell model (2.2) follows by the Lax–Milgram lemma.

3. The mesh (stent) model. We consider general three-dimensional mesh-like elastic objects, which can be used to reinforce a given shell surface. A motivating example for this work is a medical device called a stent. A stent is a metallic mesh-like tube that is inserted into a clogged vessel to prop it open and help recover normal blood circulation, see Figure 1. We consider the supporting mesh structure to be a three-dimensional elastic body defined as a union of three-dimensional local components (e.g. stent struts), see Figure 1. The local components (such as stent struts) are slender objects whose geometric distribution and mechanical properties determine the overall, global, emergent elastic properties of mesh-like structures such as stents. After the insertion of a stent into a vessel, the stent deforms as a result of the forces acting on it. The forces come from the pressures exerted by blood flow onto the stented vessel, and from the contraction and expansion of the elastic vessel wall. In normal situations the deformation of slender stent struts inserted in the vessel is relatively small, and can therefore be modeled by the equations of three-dimensional linear elasticity. The equations of linearized elasticity defined on thin domains such as those of stent struts are computationally very expensive to solve. The discretized problem is typically ill-conditioned, and very fine discretization with large memory requirements is necessary to obtain convergent solutions. For these reasons, reduced models, based on dimension reduction, should be used/developed whenever mesh-like objects consisting of slender elastic components are considered.

This is why in this work we choose to model a mesh-like structure such as a stent as a collection of one-dimensional curved rods representing the slender mesh components, e.g., stent struts. The resulting mathematical equations are the static equilibrium equations defined on a graph domain representing the mesh (stent) geometry. Contact conditions between different graph components, i.e., slender stent struts, need to be defined to obtain a well-defined mathematical problem. The resulting reduced mesh model is "consistent" with 3D elasticity, i.e., it approximates well the full 3D model problem [16, 20, 21, 8].

3.1. 1D curved rod model. A three-dimensional elastic body with its two dimensions small compared to the third, is generally called an elastic rod, see Figure 2. A curved rod model is a one-dimensional approximation of a "thin" three-dimensional

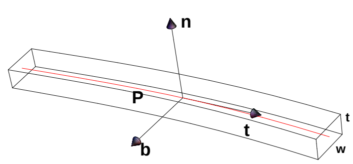

FIG. 2. *3D thin elastic body*

curved elastic structure. The model is given in terms of the arc-length of the middle curve of the rod as an unknown variable. Thus in order to build the 1D model a parametrization $\boldsymbol{P} : [0, l] \to \mathbb{R}^3$ of the middle curve of the curved rod (red in Figure 2) has to be given. To make things precise, let us assume that the cross-section of the curved rod is rectangular, of width w and thickness t. Denote by $\boldsymbol{n}$ the normal to the middle curve, perpendicular to the rod's width, and by $\boldsymbol{b}$ the binormal. See Figure 2. The one-dimensional model for curved elastic rods that we use here is given in terms of the following unknowns: $\tilde{\boldsymbol{u}}$ - middle line of the curved rod, $\tilde{\boldsymbol{\omega}}$ - infinitesimal rotation of the cross-sections, $\tilde{\boldsymbol{q}}$ - contact moment, and $\tilde{\boldsymbol{p}}$ - contact force. The model is a first-order system, where the first-order derivative $\,'$ denotes the derivative with respect to the arc length of the middle line of the curved rod. For a given force with line density $\tilde{\boldsymbol{f}}$, and angular momentum $\tilde{\boldsymbol{g}}$, the model reads: find $(\tilde{\boldsymbol{u}}, \tilde{\boldsymbol{\omega}}, \tilde{\boldsymbol{q}}, \tilde{\boldsymbol{p}})$ such that

$$\left\{ \begin{array}{ll} 0 & = \tilde{\boldsymbol{p}}' + \tilde{\boldsymbol{f}}, \\ 0 & = \tilde{\boldsymbol{q}}' + \boldsymbol{t} \times \tilde{\boldsymbol{p}} + \tilde{\boldsymbol{g}} \end{array} \right. \tag{3.1}$$

$$\left\{ \begin{array}{ll} 0 & = \tilde{\boldsymbol{\omega}}' - \mathbf{Q}\mathbf{H}^{-1}\mathbf{Q}^T \tilde{\boldsymbol{q}}, \\ 0 & = \tilde{\boldsymbol{u}}' + \boldsymbol{t} \times \tilde{\boldsymbol{\omega}}. \end{array} \right. \tag{3.2}$$

The first two equations describe the balance of contact force and contact moment, respectively, while the last two equations describe the constitutive relation for a curved, linearly elastic rod, and the condition of inextensibility and unshearability of the rod, respectively. The matrices $\mathbf{H}$ and $\mathbf{Q}$ are given by [10]:

$$\mathbf{H} = \left[\begin{array}{ccc} \mu K & 0 & 0 \\ 0 & EI_{22} & EI_{23} \\ 0 & EI_{23} & EI_{33} \end{array} \right], \qquad \mathbf{Q} = \left[\begin{array}{ccc} \boldsymbol{t} & \boldsymbol{n} & \boldsymbol{b} \end{array} \right].$$

Here $E = \mu(3\lambda + 2\mu)/(\lambda + \mu)$ is the Youngs modulus (μ and λ are the Lamé constants of the rod material), I_{ij} are the moments of inertia of the cross-sections, and μK is torsion rigidity of the cross-sections. Therefore, $\mathbf{H}$ describes the elastic properties of the rods (struts) and the geometry of the cross-sections.

This model is a linearization of the Antman-Cosserat model for inextensible, unshearable rods (see [2] for the nonlinear model and [8] for its linearization). It can also be obtained as a linearization of the model derived in [28], which is obtained from 3D nonlinear elasticity by using Γ-convergence techniques on curved rod-like hyperelastic structures. It was shown in [20] that the solution of the 1D rod model can be obtained as a limit of solutions of equilibrium equations of 3D elasticity when the thickness and width of the cross-sections t and w tend to zero together. Therefore, for 3D rods that are thin enough, the 1D curved rod model provides a good approximation of 3D elasticity. Moreover, it was shown in [30] that the curved geometry of rods, i.e., stent struts, can be approximated with a piecewise straight geometry with an error estimate. This will further simplify the equations of the 1D curved rod model.

The problem for a single rod: weak formulation. To derive a weak formulation we proceed as usual: multiply the first equation in (3.1) by $\tilde{\boldsymbol{v}}$ and the second equation in (3.1) by $\tilde{\boldsymbol{w}}$, where $(\tilde{\boldsymbol{v}}, \tilde{\boldsymbol{w}}) \in H^1(0,\ell;\mathbb{R}^3) \times H^1(0,\ell;\mathbb{R}^3)$, and integrate by parts over $[0,\ell]$. After inserting $\tilde{\boldsymbol{q}}$ from the first equation in (3.2) we obtain:

$$\begin{aligned} 0 = & -\int_0^\ell \tilde{\boldsymbol{p}} \cdot (\tilde{\boldsymbol{v}}' + \boldsymbol{t} \times \tilde{\boldsymbol{w}}) ds + \int_0^\ell \boldsymbol{f} \cdot \tilde{\boldsymbol{v}} ds - \int_0^\ell \mathbf{Q}\mathbf{H}\mathbf{Q}^T \tilde{\boldsymbol{\omega}}' \cdot \tilde{\boldsymbol{w}}' ds + \int_0^\ell \tilde{\boldsymbol{g}} \cdot \tilde{\boldsymbol{w}} ds \\ & + \tilde{\boldsymbol{p}}(\ell) \cdot \tilde{\boldsymbol{v}}(\ell) - \tilde{\boldsymbol{p}}(0) \cdot \tilde{\boldsymbol{v}}(0) + \tilde{\boldsymbol{q}}(\ell) \cdot \tilde{\boldsymbol{w}}(\ell) - \tilde{\boldsymbol{q}}(0) \cdot \tilde{\boldsymbol{w}}(0). \end{aligned}$$

The condition for inextensibility and unshearability of the curved rod, i.e., the second equation in (3.2), is included in the test space, which we define to be:

$$V = \{(\tilde{\boldsymbol{v}}, \tilde{\boldsymbol{w}}) \in H^1(0,\ell;\mathbb{R}^3) \times H^1(0,\ell;\mathbb{R}^3) : \tilde{\boldsymbol{v}}' + \boldsymbol{t} \times \tilde{\boldsymbol{w}} = 0\}.$$

The weak formulation for a single rod problem (3.1)-(3.2) is then given by: find $(\tilde{\boldsymbol{u}}, \tilde{\boldsymbol{\omega}}) \in V$ such that

$$\begin{aligned} \int_0^\ell \mathbf{Q}\mathbf{H}\mathbf{Q}^T \tilde{\boldsymbol{\omega}}' \cdot \tilde{\boldsymbol{w}}' ds = & \int_0^\ell \boldsymbol{f} \cdot \tilde{\boldsymbol{v}} ds + \int_0^\ell \tilde{\boldsymbol{g}} \cdot \tilde{\boldsymbol{w}} ds \\ & + \tilde{\boldsymbol{q}}(\ell) \cdot \tilde{\boldsymbol{w}}(\ell) - \tilde{\boldsymbol{q}}(0) \cdot \tilde{\boldsymbol{w}}(0) + \tilde{\boldsymbol{p}}(\ell) \cdot \tilde{\boldsymbol{v}}(\ell) - \tilde{\boldsymbol{p}}(0) \cdot \tilde{\boldsymbol{v}}(0), \quad \forall (\tilde{\boldsymbol{v}}, \tilde{\boldsymbol{w}}) \in V. \end{aligned} \tag{3.3}$$

For a single rod, the boundary conditions at $s = 0, \ell$ need to be prescribed. For the stent problem, the end points of each rod will correspond to stent's vertices where the stent struts (curved rods) meet. At those point the coupling conditions will have to be prescribed. In particular, it will be required that the sum of contact forces be equal to zero, and that the sum of contact moments be equal to zero, for all the rods meeting at a given vertex. This condition will take care of the boundary conditions at $s = 0, \ell$ for all the rods meeting at a given vertex.

3.2. Elastic mesh as a 3D net of 1D curved rods. We recall that a 3D elastic mesh-like structure is defined as a 3D elastic body obtained as a union of its three-dimensional slender components. The mechanical properties of each 3D stent mesh component will be modeled by the 1D curved rod model, discussed in the previous section. To pose a well-defined mathematical problem in which a mesh-like elastic structure is modeled as a union of 1D curved rods, we need to define the (topological) distribution of slender rods, the rods' geometry, the points were the slender rods meet, the mechanical properties of the rod's material, and the coupling conditions, i.e., the mechanics of the interaction between the slender components at the points where they meet. Thus, we need to prescribe:

- $\mathcal{V}$ - a set of mesh vertices (i.e., the points where middle lines of curved rods meet),
- $\mathcal{N}$ - a set of mesh edges (i.e., the pairing of vertices),
- $\boldsymbol{P}^i$ - a parametrization of the middle line of the ith rod (i.e., of the edge $e_i \in \mathcal{N}$),
- ρ_i, μ_i, E_i - the material constants of the ith rod,
- w^i, t^i - the width and thickness of the cross-section of the ith rod,
- The coupling conditions at each vertex $\boldsymbol{V}$ in $\mathcal{V}$.

Note that $(\mathcal{V}, \mathcal{N})$ defines a graph and sets the topology of the mesh net. Defining the precise geometry of each slender rod, e.g., defining whether the slender rod component is curved or straight, is given by parameterization $\boldsymbol{P}^i$ of the middle line. This introduces orientation in the graph. The weak formulation of the elastic mesh net problem, defined below, is independent of the choice of orientation of its slender components. For each edge $e_i \in \mathcal{N}$, the following 1D curved rod model is used to describe the 3D mechanical properties of the ith slender mesh component:

$$0 = \tilde{\boldsymbol{p}}^{i\prime} + \tilde{\boldsymbol{f}}^i, \tag{3.4}$$

$$0 = \tilde{\boldsymbol{q}}^{i\prime} + \boldsymbol{t}^i \times \tilde{\boldsymbol{p}}^i + \tilde{\boldsymbol{g}}^i, \tag{3.5}$$

$$0 = \tilde{\boldsymbol{\omega}}^{i\prime} - \mathbf{Q}^i(\mathbf{H}^i)^{-1}(\mathbf{Q}^i)^T\tilde{\boldsymbol{q}}^i, \tag{3.6}$$

$$0 = \tilde{\boldsymbol{u}}^{i\prime} + \boldsymbol{t}^i \times \tilde{\boldsymbol{\omega}}^i. \tag{3.7}$$

At each vertex $\boldsymbol{V} \in \mathcal{V}$, two coupling conditions need to be satisfied for all the edges meeting at vertex $\boldsymbol{V}$:

- the **kinematic coupling condition** requiring continuity of middle lines and infinitesimal rotation of cross-sections for all the rods meeting at $\boldsymbol{V}$, i.e., $(\tilde{\boldsymbol{u}}, \tilde{\boldsymbol{\omega}})$ must be continuous at each vertex,
- the **dynamic coupling condition** requiring the balance of contact forces $(\tilde{\boldsymbol{p}})$ and contact moments $(\tilde{\boldsymbol{q}})$ at each vertex.

Weak formulation for the elastic mesh problem. We begin by first defining a function space $H^1_c(\mathcal{N}; \mathbb{R}^k)$ which is defined on a mesh net $(\mathcal{V}, \mathcal{N})$. This space will be used in the definition of the test space for the elastic mesh net problem. The space

$H^1_c(\mathcal{N};\mathbb{R}^k)$ consists of all the H^1-functions $\tilde{\boldsymbol{u}}_S$,

$$\tilde{\boldsymbol{u}}_S = ((\tilde{\boldsymbol{u}}^1, \tilde{\boldsymbol{\omega}}^1), \ldots, (\tilde{\boldsymbol{u}}^{n_E}, \tilde{\boldsymbol{\omega}}^{n_E})), \quad \text{where } (\tilde{\boldsymbol{u}}^i, \tilde{\boldsymbol{\omega}}^i) \text{ is defined on edge } e^i, i = 1, , n_E,$$

such that the kinematic coupling condition is satisfied at each vertex $\boldsymbol{V} \in \mathcal{V}$. More precisely, at each vertex $\boldsymbol{V} \in \mathcal{V}$ at which the edges $\boldsymbol{e}^i$ and $\boldsymbol{e}^j$ meet, the kinematic condition says that the trace of $(\tilde{\boldsymbol{u}}^i, \tilde{\boldsymbol{\omega}}^i)$ at $s \in \{0, \ell^i\}$ that corresponds to vertex $\boldsymbol{V}$, i.e., $(\tilde{\boldsymbol{u}}^i, \tilde{\boldsymbol{\omega}}^i)((\boldsymbol{P}^i)^{-1}(\boldsymbol{V}))$, has to be equal to the trace $(\tilde{\boldsymbol{u}}^j, \tilde{\boldsymbol{\omega}}^j)((\boldsymbol{P}^j)^{-1}(\boldsymbol{V}))$. Thus, for $k \in \mathbb{N}$, we define

$$H^1_c(\mathcal{N};\mathbb{R}^k) = \Big\{ \tilde{\boldsymbol{u}}_S = ((\tilde{\boldsymbol{u}}^1, \tilde{\boldsymbol{\omega}}^1), \ldots, (\tilde{\boldsymbol{u}}^{n_E}, \tilde{\boldsymbol{\omega}}^{n_E})) \in \prod_{i=1}^{n_E} H^1(0, \ell^i; \mathbb{R}^k) :$$
$$(\tilde{\boldsymbol{u}}^i, \tilde{\boldsymbol{\omega}}^i)((\boldsymbol{P}^i)^{-1}(\boldsymbol{V})) = (\tilde{\boldsymbol{u}}^j, \tilde{\boldsymbol{\omega}}^j)((\boldsymbol{P}^j)^{-1}(\boldsymbol{V})), \ \forall \boldsymbol{V} \in \mathcal{V}, \boldsymbol{V} \in \boldsymbol{e}^i \cap \boldsymbol{e}^j \Big\}.$$

A natural norm for this space is given by

$$\|\tilde{\boldsymbol{u}}_S\|^2_{H^1_c(\mathcal{N};\mathbb{R}^k)} = \sum_{i=1}^{n_E} \left(\|\tilde{\boldsymbol{u}}^i\|^2_{H^1(0,\ell^i;\mathbb{R}^k)} + \|\tilde{\boldsymbol{\omega}}^i\|^2_{H^1(0,\ell^i;\mathbb{R}^k)} \right).$$

The test space V_s for the elastic mesh net problem is then defined to be the subspace of $H^1_c(\mathcal{N}, \mathbb{R}^k)$ such that the inextensibility and unshearability conditions are satisfied. More precisely, we define the test space for the elastic mesh net problem to be

$$V_S = \{\tilde{\boldsymbol{v}}_S = ((\tilde{\boldsymbol{v}}^1, \tilde{\boldsymbol{w}}^1), \ldots, (\tilde{\boldsymbol{v}}^{n_E}, \tilde{\boldsymbol{w}}^{n_E})) \in H^1_c(\mathcal{N};\mathbb{R}^6) \colon \tilde{\boldsymbol{v}}^{i\prime} + \boldsymbol{t}^i \times \tilde{\boldsymbol{w}}^i = 0, i = 1, \ldots, n_E\}.$$

The inclusion of the kinematic coupling condition into the test space states that all possible candidates for the solution must satisfy the continuity of displacement and continuity of infinitesimal rotation, thereby avoiding the case of disconnection of mesh components or mesh rupture, which would be described by a jump in displacement or infinitesimal rotation of a cross-section, in which case the model equations cease to be valid. The kinematic coupling condition is required to be satisfied in the strong sense. The dynamic coupling conditions, however, will be satisfied in weak sense by imposing the condition in the weak formulation of the underlying equations, which are obtained as follows. Since an elastic mesh structure is defined as a union of slender rod components, i.e., curved rods, the weak formulation is obtained as a sum of weak formulations for each curved rod $e_i, i = 1, \cdots, n_E$. By the dynamic contact conditions the boundary terms involving $\tilde{\boldsymbol{p}}$, and the boundary terms involving $\tilde{\boldsymbol{q}}$ that come from the right hand-sides of equations (3.3) for $i = 1, , n_E$, will all sum up to zero. This is because the dynamic contact conditions state that the sum of contact forces is zero, and the sum of contact moments at each vertex must be zero, i.e., the contact forces are exactly balanced, and contact moments are exactly balanced at each vertex. The resulting weak formulation then reads as follows: find $\tilde{\boldsymbol{u}}_S = ((\tilde{\boldsymbol{u}}^1, \tilde{\boldsymbol{\omega}}^1), \ldots, (\tilde{\boldsymbol{u}}^{n_E}, \tilde{\boldsymbol{\omega}}^{n_E})) \in V_S$ such that

$$\sum_{i=1}^{n_E} \int_0^{\ell^i} \mathbf{Q}^i \mathbf{H}^i {\mathbf{Q}^i}^T \tilde{\boldsymbol{\omega}}^{i\prime} \cdot \tilde{\boldsymbol{w}}^{i\prime} ds = \sum_{i=1}^{n_E} \int_0^{\ell^i} \tilde{\boldsymbol{f}}^i \cdot \tilde{\boldsymbol{v}}^i ds + \sum_{i=1}^{n_E} \int_0^{\ell^i} \tilde{\boldsymbol{g}}^i \cdot \tilde{\boldsymbol{w}}^i ds \tag{3.8}$$

holds for all the test function $\tilde{\boldsymbol{v}}_S = ((\tilde{\boldsymbol{v}}^1, \tilde{\boldsymbol{w}}^1), \ldots, (\tilde{\boldsymbol{v}}^{n_E}, \tilde{\boldsymbol{w}}^{n_E})) \in V_S$.

To simplify notation further in the text, we introduce the following notation for the bi-linear form appearing on the left hand-side of the weak formulation (3.8):

$$a_{\mathrm{mesh}}(\tilde{\boldsymbol{u}}_S, \tilde{\boldsymbol{v}}_S) := \sum_{i=1}^{n_E} \int_0^{\ell^i} \mathbf{Q}^i \mathbf{H}^i \mathbf{Q}^{i^T} \tilde{\boldsymbol{\omega}}^{i\prime} \cdot \tilde{\boldsymbol{w}}^{i\prime} ds. \tag{3.9}$$

In terms of this notation, the weak formulation of our elastic mesh net problem reads: find $\tilde{\boldsymbol{u}}_S = ((\tilde{\boldsymbol{u}}^1, \tilde{\boldsymbol{\omega}}^1), \dots, (\tilde{\boldsymbol{u}}^{n_E}, \tilde{\boldsymbol{\omega}}^{n_E})) \in V_S$ such that

$$a_{\mathrm{mesh}}(\tilde{\boldsymbol{u}}_S, \tilde{\boldsymbol{v}}_S) = \sum_{i=1}^{n_E} \int_0^{\ell^i} \tilde{\boldsymbol{f}}^i \cdot \tilde{\boldsymbol{v}}^i ds + \sum_{i=1}^{n_E} \int_0^{\ell^i} \tilde{\boldsymbol{g}}^i \cdot \tilde{\boldsymbol{w}}^i ds$$

holds for all the test function $\tilde{\boldsymbol{v}}_S = ((\tilde{\boldsymbol{v}}^1, \tilde{\boldsymbol{w}}^1), \dots, (\tilde{\boldsymbol{v}}^{n_E}, \tilde{\boldsymbol{w}}^{n_E})) \in V_S$.

More details about the model can be found in [8]. Starting from 3D linearized elasticity, the 1D reduced model defined as a collection of 1D rods was rigorously derived and justified in [16].

The following estimate, which holds for the elastic mesh net problem, will be useful later in the analysis of the coupled mesh-reinforced shell model.

Lemma 3.1. *There exists a constant $C_{\mathrm{mesh}} > 0$ such that*

$$\begin{aligned} a_{\mathrm{mesh}}(\tilde{\boldsymbol{u}}_S, \tilde{\boldsymbol{u}}_S) &+ \sum_{i=1}^{n_E} \|\tilde{\boldsymbol{\omega}}^i\|^2_{L^2(0,\ell^i;\mathbb{R}^3)} \\ &\geq C_{\mathrm{mesh}} \sum_{i=1}^{n_E} (\|(\tilde{\boldsymbol{\omega}}^i)'\|^2_{L^2(0,\ell^i;\mathbb{R}^3)} + \|(\tilde{\boldsymbol{u}}^i)'\|^2_{L^2(0,\ell^i;\mathbb{R}^3)}), \; (\tilde{\boldsymbol{u}}_S, \tilde{\boldsymbol{\omega}}_S) \in V_S. \end{aligned}$$

Proof. The estimate of the right hand-side implies (with $\mathbf{H}^i$ positive definite)

$$\begin{aligned} &\sum_{i=1}^{n_E} (\|(\tilde{\boldsymbol{\omega}}^i)'\|^2_{L^2(0,\ell^i;\mathbb{R}^3)} + \|(\tilde{\boldsymbol{u}}^i)'\|^2_{L^2(0,\ell^i;\mathbb{R}^3)}) \\ &\leq \sum_{i=1}^{n_E} (\|(\tilde{\boldsymbol{\omega}}^i)'\|^2_{L^2(0,\ell^i;\mathbb{R}^3)} + 2\|(\tilde{\boldsymbol{u}}^i)' + \boldsymbol{t}^i \times \tilde{\boldsymbol{\omega}}^i\|^2_{L^2(0,\ell^i;\mathbb{R}^3)} + 2\|\boldsymbol{t}^i \times \tilde{\boldsymbol{\omega}}^i\|^2_{L^2(0,\ell^i;\mathbb{R}^3)}) \\ &\leq \sum_{i=1}^{n_E} \left(\int_0^{\ell^i} (\tilde{\boldsymbol{\omega}}^i)' \cdot (\tilde{\boldsymbol{\omega}}^i)' ds + 2\|\tilde{\boldsymbol{\omega}}^i\|^2_{L^2(0,\ell^i;\mathbb{R}^3)} \right) \\ &\leq \sum_{i=1}^{n_E} \left(\frac{1}{\min \sigma(\mathbf{H}^i)} \int_0^{\ell^i} \mathbf{Q}^i \mathbf{H}^i \mathbf{Q}^{i^T} (\tilde{\boldsymbol{\omega}}^i)' \cdot (\tilde{\boldsymbol{\omega}}^i)' ds + 2\|\tilde{\boldsymbol{\omega}}^i\|^2_{L^2(0,\ell^i;\mathbb{R}^3)} \right) \\ &\leq \frac{1}{\min_i \min \sigma(\mathbf{H}^i)} a_{\mathrm{mesh}}(\tilde{\boldsymbol{u}}_S, \tilde{\boldsymbol{u}}_S) + 2 \sum_{i=1}^{n_E} \|\tilde{\boldsymbol{\omega}}^i\|^2_{L^2(0,\ell^i;\mathbb{R}^3)}. \end{aligned}$$

This implies the statement of the lemma. ∎

4. The coupled mesh-reinforced shell model.

We are interested in studying the coupled mesh-reinforced shell model, where the mesh and the shell are fixed or "glued" to each other.

4.1. Formulation of the coupled problem.

We begin by recalling that in Section 2 we introduced a Naghdi shell parameterized by $\boldsymbol{\varphi} : \overline{\omega} \to \mathbb{R}^3$, and in Section 3 we introduced an elastic mesh net model, where the slender rod components are parameterized by $\boldsymbol{P}^i : [0, \ell^i] \to \mathbb{R}^3$. We assume that the shell and the reinforcing mesh are in "perfect contact", without slip, affixed one to another, so that the following holds:

$$\bigcup_{i=1}^{n_E} \boldsymbol{P}^i([0,\ell^i]) \subset S = \boldsymbol{\varphi}(\overline{\omega}).$$

See Figure 3. We assume that $\boldsymbol{\varphi}$ is injective on ω. Therefore the functions

$$\boldsymbol{\pi}^i := \boldsymbol{\varphi}^{-1} \circ \boldsymbol{P}^i : [0,\ell^i] \to \overline{\omega}, \qquad i = 1, \dots n_E$$

are well defined. The functions $\boldsymbol{\pi}^i$ define the reparameterization of slender rods from the interval domain $[0, \ell^i]$ to the shell parameter domain $\overline{\omega}$.

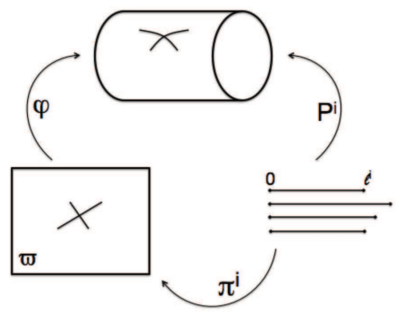

FIG. 3. *Reparameterization of stent struts.*

We next show that if the Naghdi shell parameterization $\boldsymbol{\varphi}$ is C^1, then the reparametererizations $\boldsymbol{\pi}^i$ of stent struts are non-degenerate in the sense that $\|(\boldsymbol{\pi}^i)'(s)\|$ is aways uniformly bounded away from zero. More precisely, we have:

LEMMA 4.1. *Let $\boldsymbol{\varphi} \in C^1(\overline{\omega}; \mathbb{R}^3)$. Then there exists a $c_\pi > 0$ such that*

$$c_\pi \le \|(\boldsymbol{\pi}^i)'(s)\|, \qquad s \in [0, \ell^i], i = 1, \dots, n_E.$$

Proof. From the definition we obtain $\boldsymbol{\varphi}(\boldsymbol{\pi}^i) = \boldsymbol{P}^i$ for each $i = 1, \dots, n_E$. Thus

$$\nabla \boldsymbol{\varphi}(\boldsymbol{\pi}^i(s))(\boldsymbol{\pi}^i)'(s) = (\boldsymbol{P}^i)'(s), \qquad s \in [0, \ell^i].$$

Since $\boldsymbol{P}^i$ is the natural parametrization one has

$$1 = \|(\boldsymbol{P}^i)'(s)\| \le \|\nabla \boldsymbol{\varphi}(\boldsymbol{\pi}^i(s))\|_F \|(\boldsymbol{\pi}^i)'(s)\|, \qquad s \in [0,\ell^i], i = 1, \dots, n_E,$$

where $\|\cdot\|$ is the Euclidean norm and $\|\cdot\|_F$ is the Frobenius norm. Therefore, since $\nabla\boldsymbol{\varphi}$ is continuous and regular on the compact set $\overline{\omega}$, we obtain that

$$0 < c_\pi = \frac{1}{\sup_{x \in \overline{\omega}} \|\nabla \boldsymbol{\varphi}(x)\|_F} \le \|(\boldsymbol{\pi}^i)'(s)\|, \qquad s \in [0,\ell^i], i = 1, \dots, n_E.$$

The weak formulation of the coupled problem. To define the weak formulation of the coupled problem we introduce the following function space:

$$V_{\text{coupled}} = \{(\boldsymbol{v}, \boldsymbol{w}) \in V_N(\omega) : ((\boldsymbol{v} \circ \pi^1, \boldsymbol{w} \circ \pi^1), \dots, (\boldsymbol{v} \circ \pi^{n_E}, \boldsymbol{w} \circ \pi^{n_E})) \in V_S\}, \tag{4.1}$$

where we recall that $V_N(\omega)$ and V_S are the corresponding function spaces for the weak solution of the Naghdi shell and the elastic mesh problem, respectively. Thus, the function space for the coupled problem consists of all the functions $(\boldsymbol{v},\boldsymbol{w}) \in V_N(\omega)$, i.e., all the displacements $\boldsymbol{v}$ and all the infinitesimal rotations $\boldsymbol{w}$ in $V_N(\omega)$, such that the composite function

$$(\boldsymbol{v},\boldsymbol{w})\circ\boldsymbol{\pi} = ((\boldsymbol{v}\circ\pi^1,\boldsymbol{w}\circ\pi^1),\ldots,(\boldsymbol{v}\circ\pi^{n_E},\boldsymbol{w}\circ\pi^{n_E})),$$

i.e., the $\boldsymbol{\pi}$-reparameterization, belongs to the mesh net solution space V_S. Notice that this imposes additional regularity on the functions in the Naghdi shell space $V_N(\omega)$.

Lemma 4.2. *The function space V_{coupled} is complete, equipped with the norm*

$$\|(\boldsymbol{v},\boldsymbol{w})\|_{V_{\text{coupled}}} = \left(\|(\boldsymbol{v},\boldsymbol{w})\|^2_{V_N(\omega)} + \|(\boldsymbol{v},\boldsymbol{w})\circ\boldsymbol{\pi}\|^2_{H^1_c(\mathcal{N};\mathbb{R}^6)}\right)^{1/2}.$$

Proof. To see that this is a norm on V_{coupled} is obvious. Thus we only have to show completeness. For this purpose assume that $((\boldsymbol{u}^n,\boldsymbol{\omega}^n))_n \subset V_{\text{coupled}}$ is a Cauchy sequence in V_{coupled}. Therefore $((\boldsymbol{u}^n,\boldsymbol{\omega}^n))_n$ is a Cauchy sequence in $V_N(\omega)$ and

$$(\boldsymbol{u}^n\circ\boldsymbol{\pi}^i)_n, (\boldsymbol{\omega}^n\circ\boldsymbol{\pi}^i)_n \subseteq H^1(0,\ell^i;\mathbb{R}^3), \qquad i=1,\ldots n_E$$

are Cauchy sequences in $H^1(0,\ell^i;\mathbb{R}^3)$. Since $V_N(\omega)$ and $H^1(0,\ell^i;\mathbb{R}^3)$ are complete we obtain the following convergence properties

$$\begin{aligned} &(\boldsymbol{u}^n,\boldsymbol{\omega}^n)\to(\boldsymbol{u},\boldsymbol{\omega}) \quad \text{in } V_N(\omega),\\ &\boldsymbol{u}^n\circ\boldsymbol{\pi}^i\to\tilde{\boldsymbol{u}}^i, \boldsymbol{\omega}^n\circ\boldsymbol{\pi}^i\to\tilde{\boldsymbol{\omega}}^i \quad \text{in } H^1(0,\ell^i;\mathbb{R}^3), i=1,\ldots,n_E. \end{aligned} \tag{4.2}$$

From the properties of the trace operator and the first convergence in (4.2) we obtain $\tilde{\boldsymbol{u}}^i = \boldsymbol{u}\circ\boldsymbol{\pi}^i$, $\tilde{\boldsymbol{\omega}}^i = \boldsymbol{\omega}\circ\boldsymbol{\pi}^i$, for all $i=1,\ldots,n_E$. Now, by using the second convergence in (4.2) we can take the limits in the inextensibility and unshearability conditions:

$$(\boldsymbol{u}^n\circ\boldsymbol{\pi}^i)' + \boldsymbol{t}^i\times\boldsymbol{\omega}^n\circ\boldsymbol{\pi}^i = 0$$

to obtain that the limit function $(\boldsymbol{u}\circ\boldsymbol{\pi}^i,\boldsymbol{\omega}\circ\boldsymbol{\pi}^i)$ satisfies the same equation and thus $(\boldsymbol{u},\boldsymbol{\omega})\circ\boldsymbol{\pi}$ belongs to V_S. Therefore, completeness is proved. ∎

To define the weak formulation of the coupled problem we introduce the following bilinear form on V_{coupled}:

$$a_{\text{coupled}}((\boldsymbol{u},\boldsymbol{\omega}),(\boldsymbol{v},\boldsymbol{w})) := a_{\text{shell}}((\boldsymbol{u},\boldsymbol{\omega}),(\boldsymbol{v},\boldsymbol{w})) + a_{\text{mesh}}((\boldsymbol{u},\boldsymbol{\omega})\circ\boldsymbol{\pi},(\boldsymbol{v},\boldsymbol{w})\circ\boldsymbol{\pi})$$

and the linear functional containing the loads:

$$l((\boldsymbol{v},\boldsymbol{w})) := \int_\omega \boldsymbol{f}\cdot\boldsymbol{v}\,dx.$$

The model is now deduced from energy consideration. Namely, the total energy of the coupled system is the sum of the potential energies of the shell and of the stent, plus the work done by the loads exerted onto the shell. Therefore, the total energy of the coupled system is equal to

$$J_{\text{coupled}}: V_{\text{coupled}}\to\mathbb{R}, \qquad J_{\text{coupled}}((\boldsymbol{v},\boldsymbol{w})) := \frac{1}{2}a_{\text{coupled}}((\boldsymbol{v},\boldsymbol{w}),(\boldsymbol{v},\boldsymbol{w})) - l((\boldsymbol{v},\boldsymbol{w})). \tag{4.3}$$

The equilibrium problem for the coupled system can be now given by the minimization problem: find $(\boldsymbol{u},\boldsymbol{\omega}) \in V_{\text{coupled}}$ such that

$$J_{\text{coupled}}((\boldsymbol{u},\boldsymbol{\omega})) = \min_{(\boldsymbol{v},\boldsymbol{w})\in V_{\text{coupled}}} J_{\text{coupled}}((\boldsymbol{v},\boldsymbol{w})). \tag{4.4}$$

For a symmetric bilinear form a_{coupled} one simply obtains (e.g. see [11, Theorem 6.3-2]) that the minimization problem is equivalent to the following weak formulation: find $(\boldsymbol{u},\boldsymbol{\omega}) \in V_{\text{coupled}}$ such that

$$a_{\text{coupled}}((\boldsymbol{u},\boldsymbol{\omega}),(\boldsymbol{v},\boldsymbol{w})) = l((\boldsymbol{v},\boldsymbol{w})), \qquad \forall(\boldsymbol{v},\boldsymbol{w}) \in V_{\text{coupled}}. \tag{4.5}$$

More precisely, by taking into account the definition of a_{coupled} and l, one obtaines the following weak formulation of the coupled problem: find $(\boldsymbol{u},\boldsymbol{\omega}) \in V_{\text{coupled}}$, where V_{coupled} is given in (4.1), such that

$$\begin{aligned}
&h\int_\omega \mathbf{Q}\mathcal{C}_m(\mathbf{Q}^T\left[\begin{array}{cc} \partial_1\boldsymbol{u}+\boldsymbol{a}_1\times\boldsymbol{\omega} & \partial_2\boldsymbol{u}+\boldsymbol{a}_2\times\boldsymbol{\omega}\end{array}\right]) \\
&\qquad\qquad\qquad \cdot\left[\begin{array}{cc} \partial_1\boldsymbol{v}+\boldsymbol{a}_1\times\boldsymbol{w} & \partial_2\boldsymbol{v}+\boldsymbol{a}_2\times\boldsymbol{w}\end{array}\right]\sqrt{a}dx \\
&+\frac{h^3}{12}\int_\omega \mathbf{Q}\mathcal{C}_f(\mathbf{Q}^T\nabla\boldsymbol{\omega})\cdot\nabla\boldsymbol{w}\sqrt{a}dx + \sum_{i=1}^{n_E}\int_0^{\ell^i} \mathbf{Q}^i\mathbf{H}^i{\mathbf{Q}^i}^T(\boldsymbol{\omega}\circ\boldsymbol{\pi}^i)'\cdot(\boldsymbol{w}\circ\boldsymbol{\pi}^i)'ds \\
&=\int_\omega \boldsymbol{f}\cdot\boldsymbol{v}dx
\end{aligned} \tag{4.6}$$

holds for all $(\boldsymbol{v},\boldsymbol{w}) \in V_{\text{coupled}}$.

Here, the properties of the material and of the cross-sections of the mesh rod components are described by the tensor $\mathbf{H}^i$, while the local basis attached to each rod is captured by $\mathbf{Q}^i$. The local basis associated with the shell is given in $\mathbf{Q}$, while the elastic properties of the shell are given by the elasticity tensors $\mathcal{C}_m$ and $\mathcal{C}_f$, see (2.3).

4.2. Existence of a unique solution to the coupled mesh-reinforced shell problem.

THEOREM 4.3. *There exists a unique solution to the minimization problem (4.4), and thus, there exists a unique weak solution to the coupled mesh-reinforced shell problem (4.5).*

Proof. The proof follows from the Lax-Milgram lemma. More precisely, since V_{coupled} is complete by Lemma 4.2, and the functionals in (4.5) are obviously continuous on V_{coupled}, one only needs to prove that the form a_{coupled} is V_{coupled}–elliptic. For that purpose, we estimate $a_{\text{coupled}}((\boldsymbol{u},\boldsymbol{\omega}),(\boldsymbol{u},\boldsymbol{\omega}))$ for $(\boldsymbol{u},\boldsymbol{\omega}) \in V_{\text{coupled}}$ by using the positive definiteness of a_{shell}, a_{mesh} and the property of the trace on $V_N(\omega)$. More precisely, from the positive definiteness of a_{shell}, given by the estimate (2.6), and from trace property on $V_N(\omega)$, we first have:

$$\begin{aligned}
a_{\text{coupled}}((\boldsymbol{u},\boldsymbol{\omega}),(\boldsymbol{u},\boldsymbol{\omega})) =&\ a_{\text{shell}}((\boldsymbol{u},\boldsymbol{\omega}),(\boldsymbol{u},\boldsymbol{\omega})) + a_{\text{mesh}}((\boldsymbol{u},\boldsymbol{\omega})\circ\boldsymbol{\pi},(\boldsymbol{u},\boldsymbol{\omega})\circ\boldsymbol{\pi}) \\
&\geq C_{\text{shell}}\|(\boldsymbol{u},\boldsymbol{\omega})\|_{V_N(\omega)} + a_{\text{mesh}}((\boldsymbol{u},\boldsymbol{\omega})\circ\boldsymbol{\pi},(\boldsymbol{u},\boldsymbol{\omega})\circ\boldsymbol{\pi}) \\
&\geq c\|(\boldsymbol{u},\boldsymbol{\omega})\|_{V_N(\omega)} + c\sum_{i=1}^{n_E}(\|\boldsymbol{u}\|^2_{L^2(\boldsymbol{\pi}^i([0,\ell^i]);\mathbb{R}^3)} + \|\boldsymbol{\omega}\|^2_{L^2(\boldsymbol{\pi}^i([0,\ell^i]);\mathbb{R}^3)}) \\
&\quad + a_{\text{mesh}}((\boldsymbol{u},\boldsymbol{\omega})\circ\boldsymbol{\pi},(\boldsymbol{u},\boldsymbol{\omega})\circ\boldsymbol{\pi})
\end{aligned}$$

The constant c is generic. By using the non degeneracy property of reparametrization $\boldsymbol{\pi}^i([0,\ell^i])$, given by Lemma 4.1, we express the $L^2(\boldsymbol{\pi}^i([0,\ell^i]);\mathbb{R}^3)$ norm in terms of the $L^2(0,\ell^i;\mathbb{R}^3)$ norm:

$$\|\boldsymbol{u}\|^2_{L^2(\boldsymbol{\pi}^i([0,\ell^i]);\mathbb{R}^3)} = \int_0^{\ell^i} (\boldsymbol{u}\circ\boldsymbol{\pi}^i(s))^2 \|(\boldsymbol{\pi}^i)'(s)\| ds \geq c_\pi \|\boldsymbol{u}\circ\boldsymbol{\pi}^i\|^2_{L^2(0,\ell^i;\mathbb{R}^3)}.$$

Combined with the ellipticity of a_{mesh} given by Lemma 3.1 we obtain:

$$\begin{aligned} &a_{\text{coupled}}((\boldsymbol{u},\boldsymbol{\omega}),(\boldsymbol{u},\boldsymbol{\omega})) \\ &\qquad\geq c\|(\boldsymbol{u},\boldsymbol{\omega})\|_{V_N(\omega)} + c c_\pi \sum_{i=1}^{n_E} (\|\boldsymbol{u}\circ\boldsymbol{\pi}^i\|^2_{L^2(0,\ell^i;\mathbb{R}^3)} + \|\boldsymbol{\omega}\circ\boldsymbol{\pi}^i\|^2_{L^2(0,\ell^i;\mathbb{R}^3)}) \\ &\qquad\quad + a_{\text{mesh}}((\boldsymbol{u},\boldsymbol{\omega})\circ\boldsymbol{\pi},(\boldsymbol{u},\boldsymbol{\omega})\circ\boldsymbol{\pi}) \\ &\qquad\geq c\|(\boldsymbol{u},\boldsymbol{\omega})\|_{V_N(\omega)} + c \sum_{i=1}^{n_E} (\|\boldsymbol{u}\circ\boldsymbol{\pi}^i\|^2_{L^2(0,\ell^i;\mathbb{R}^3)} + \|\boldsymbol{\omega}\circ\boldsymbol{\pi}^i\|^2_{L^2(0,\ell^i;\mathbb{R}^3)}) \\ &\qquad\quad + c C_{\text{mesh}} \sum_{i=1}^{n_E} (\|(\boldsymbol{\omega}\circ\boldsymbol{\pi}^i)'\|^2_{L^2(0,\ell^i;\mathbb{R}^3)} + \|(\boldsymbol{u}\circ\boldsymbol{\pi}^i)'\|^2_{L^2(0,\ell^i;\mathbb{R}^3)}). \end{aligned}$$

This shows the V_{coupled}–ellipticity of the form a_{coupled}, and therefore, the existence of a unique solution to the coupled problem (4.5) by the Lax–Milgram lemma. ∎

4.3. Differential formulation of the coupled model. To obtain the differential formulation of the coupled mesh-reinforced shell problem we start by introducing a mixed weak formulation associated with the inextensibility condition in V_{coupled}. We will be assuming that the mixed weak formulation is equivalent to the weak formulation (4.6), an issue that will be discussed elsewhere, and derive the differential formulation from the equivalent mixed formulation, which we now introduce.

The mixed weak formulation. Let $Q = L^2(\mathcal{N};\mathbb{R}^3)$ and $V_{\text{mixed}} = \{(\boldsymbol{v},\boldsymbol{w}) \in V_N(\omega) : (\boldsymbol{v},\boldsymbol{w})\circ\boldsymbol{\pi} \in H^1_c(\mathcal{N};\mathbb{R}^6)\}$. The mixed formulation is then given by: find $(\boldsymbol{u},\boldsymbol{\omega},\tilde{\boldsymbol{p}}) \in V_{\text{mixed}} \times Q$, such that

$$\begin{aligned} &a_{\text{coupled}}((\boldsymbol{u},\boldsymbol{\omega}),(\boldsymbol{v},\boldsymbol{w})) + b(\tilde{\boldsymbol{p}},(\boldsymbol{v},\boldsymbol{w})\circ\boldsymbol{\pi}) = l((\boldsymbol{v},\boldsymbol{w})), \qquad \forall(\boldsymbol{v},\boldsymbol{w}) \in V_{\text{mixed}}, \\ &b(\tilde{\boldsymbol{r}},(\boldsymbol{u},\boldsymbol{\omega})\circ\boldsymbol{\pi}) = 0, \qquad \forall\tilde{\boldsymbol{r}} \in Q, \end{aligned} \tag{4.7}$$

where

$$b(\tilde{\boldsymbol{r}},(\tilde{\boldsymbol{v}},\tilde{\boldsymbol{w}})) := \sum_{i=1}^{n_E} \int_0^{\ell^i} \tilde{\boldsymbol{r}} \cdot (\tilde{\boldsymbol{v}}^{i\prime} + \boldsymbol{t}^i \times \tilde{\boldsymbol{w}}^i) ds$$

is associated with the inextensibility conditions

$$0 = \tilde{\boldsymbol{u}}^{i\prime} + \boldsymbol{t}^i \times \tilde{\boldsymbol{\omega}}^i, \qquad i = 1,\dots,n_E. \tag{4.8}$$

Notice that $\tilde{\boldsymbol{p}}$ acts as a Lagrange multiplier for the inextensibility and unshearability condition in V_S. As we shall see below, $\tilde{\boldsymbol{p}}\circ\boldsymbol{\pi}^i$ will correspond to the contact force in the mesh problem. Thus, the contact force associated with the elastic mesh components acts as the Lagrange multiplier for the stent's inextensibility and unshearability condition in the coupled mesh-shell problem (i.e., stent-vessel) problem.

Let us introduce the following notation:

$$
(4.9)\qquad
\begin{aligned}
\text{Shell}:\quad & \begin{aligned}
\mathbf{p} &= h\mathbf{Q}\mathcal{C}_m(\mathbf{Q}^T \begin{bmatrix} \partial_1 \boldsymbol{u} + \boldsymbol{a}_1 \times \boldsymbol{\omega} & \partial_2 \boldsymbol{u} + \boldsymbol{a}_2 \times \boldsymbol{\omega} \end{bmatrix}),\\
\mathbf{q} &= \frac{h^3}{12}\mathbf{Q}\mathcal{C}_f\mathbf{Q}^T \nabla \boldsymbol{\omega},
\end{aligned}\\
\text{Stent}:\quad & \begin{aligned}
\tilde{\boldsymbol{p}}^i &= \tilde{\boldsymbol{p}} \circ \boldsymbol{\pi}^i,\ \ i = 1,\dots,n_E,\\
\tilde{\boldsymbol{q}}^i &= \mathbf{Q}^i \mathbf{H}^i {\mathbf{Q}^i}^T (\boldsymbol{\omega} \circ \boldsymbol{\pi}^i)'.
\end{aligned}
\end{aligned}
$$

These new variables have physical meaning: $\mathbf{p}$ corresponds to the shell's force stress tensor (associated with the balance of linear momentum of any shell part), $\mathbf{q}$ corresponds to the so called shell's couple stress tensor (associated with the balance of angular momentum of any shell part), while $\tilde{\boldsymbol{p}}^i$ and $\tilde{\boldsymbol{q}}^i$ correspond to the mesh's force and couple vector, associated with the linear and angular momentum of each slender rod $i = 1,\dots,n_E$. Equations (4.9) describe the **constitutive equations** for the shell and mesh problem.

Now, the first equation in (4.7) can be written as

$$
(4.10)\qquad
\begin{aligned}
&\int_\omega \mathbf{p} \cdot \begin{bmatrix} \partial_1 \boldsymbol{v} + \boldsymbol{a}_1 \times \boldsymbol{w} & \partial_2 \boldsymbol{v} + \boldsymbol{a}_2 \times \boldsymbol{w} \end{bmatrix} \sqrt{a} dx + \int_\omega \mathbf{q} \cdot \nabla \boldsymbol{w} \sqrt{a} dx\\
&+ \sum_{i=1}^{n_E} \int_0^{\ell^i} \tilde{\boldsymbol{q}}^i \cdot (\boldsymbol{w} \circ \boldsymbol{\pi}^i)' ds + \sum_{i=1}^{n_E} \int_0^{\ell^i} \tilde{\boldsymbol{p}}^i \cdot ((\boldsymbol{v} \circ \boldsymbol{\pi}^i)' + \boldsymbol{t}^i \times \boldsymbol{w} \circ \boldsymbol{\pi}^i) ds\\
&= \int_\omega \boldsymbol{f} \cdot \boldsymbol{v} dx, \qquad \forall (\boldsymbol{v}, \boldsymbol{w}) \in V_{\text{mixed}}.
\end{aligned}
$$

To obtain the corresponding differential formulation, it is useful to write this weak formulation for the regions in ω that are bounded by the rods. For this purpose we note that domain ω is divided into a finite number of connected components by the sets $\boldsymbol{\pi}^i([0, \ell^i])$, which correspond to the reparameterization of slender rods in ω. We denote those connected sets by $\omega^j, j = 1,\dots,n_c$, so that

$$
\omega \backslash \bigcup_{i=1}^{n_E} \boldsymbol{\pi}^i([0, \ell^i]) = \cup_{j=1}^{n_c} \omega^j.
$$

If we now consider (4.10) for all the test functions $(\boldsymbol{v}, \boldsymbol{w}) \in V_{\text{mixed}}$ such that the support of $(\boldsymbol{v}, \boldsymbol{w})$ is in one ω^j, we obtain:

$$
\int_{\omega^j} \mathbf{p} \cdot \begin{bmatrix} \partial_1 \boldsymbol{v} + \boldsymbol{a}_1 \times \boldsymbol{w} & \partial_2 \boldsymbol{v} + \boldsymbol{a}_2 \times \boldsymbol{w} \end{bmatrix} \sqrt{a} dx + \int_{\omega^j} \mathbf{q} \cdot \nabla \boldsymbol{w} \sqrt{a} dx = \int_{\omega^j} \boldsymbol{f} \cdot \boldsymbol{v} dx.
$$

From this formulation, it is easy to write the equilibrium equations for the forces $\mathbf{p}^j := \mathbf{p}|_{\omega^j}$ and couples $\mathbf{q}^j := \mathbf{q}|_{\omega^j}$, defined on each shell connected component corresponding to ω^j:

$$
(4.11)\qquad \operatorname{div}(\sqrt{a}\mathbf{p}^j) + \boldsymbol{f} = 0, \qquad \operatorname{div}(\sqrt{a}\mathbf{q}^j) + \sqrt{a} \sum_{\alpha=1}^{2} \boldsymbol{a}_\alpha \times \mathbf{p}_\alpha^j = 0 \quad \text{in } \omega^j,
$$

where $\mathbf{p}_\alpha^j$ appearing in the second equation in (4.11) are the columns of $\mathbf{p}^j$. These equations, together with the two equations in the first line of (4.9) from where $\boldsymbol{u}$ and $\boldsymbol{\omega}$ can be recovered, constitute the differential formulation of the Naghdi shell model, see [33] for more details. Equations (4.11) describe the balance of linear and angular momentum, while the first two equations in (4.9) denote the constitutive relations (material properties) of the shell.

To include the presence of the reinforcing mesh, we proceed by performing integration by parts in the first two terms on the left hand-side in (4.10). Here we recall that ω can be written as the union of the sub-components ω^j, plus the boundary $\partial\omega^j$. Integration by parts on each sub-domain ω^j leads to the differential terms in the interior of ω^j, plus the boundary terms. Since balance of linear and angular momentum (4.11) hold in the interior of each ω^j, the only terms that remain are the boundary terms. Thus, we have:

$$
\begin{aligned}
&\sum_{j=1}^{n_c}\int_{\partial\omega^j}\mathbf{p}^j\boldsymbol{\nu}^j\cdot\boldsymbol{v}\sqrt{a}ds+\sum_{j=1}^{n_c}\int_{\partial\omega^j}\mathbf{q}^j\boldsymbol{\nu}^j\cdot\boldsymbol{w}\sqrt{a}ds\\
&+\sum_{i=1}^{n_E}\int_0^{\ell^i}\tilde{\boldsymbol{q}}^i\cdot(\boldsymbol{w}\circ\boldsymbol{\pi}^i)'ds+\sum_{i=1}^{n_E}\int_0^{\ell^i}\tilde{\boldsymbol{p}}^i\cdot((\boldsymbol{v}\circ\boldsymbol{\pi}^i)'+\boldsymbol{t}^i\times\boldsymbol{w}\circ\boldsymbol{\pi}^i)ds=0,\\
&\qquad(\boldsymbol{v},\boldsymbol{w})\in V_{\text{mixed}}.
\end{aligned}
\tag{4.12}
$$

Here $\boldsymbol{\nu}^j$ is the unit outer normal at the boundary of ω^j and the integrals over $\partial\omega^j$ are line integrals. Here we explicitly see how the contact forces coming from the shell's linear and angular momentum terms defined on $\partial\omega^j$ influence the elastic properties of the reinforcing mesh.

Now, each edge e^i is an edge for exactly two components, denote them by ω^{j_1} and ω^{j_2}. The equations on the edges that follow from (4.12) are local and can thus be decoupled. By using the change of variables in the first two integrals in (4.12) to convert the integrals over $\partial\omega^j$ into the integrals over $(0,\ell^i)$, we can write (4.12) for each edge e^i as follows:

$$
\begin{aligned}
&\int_0^{\ell^i}\mathbf{p}^{j_1}\circ\boldsymbol{\pi}^i\boldsymbol{\nu}^{j_1}\circ\boldsymbol{\pi}^i\cdot\boldsymbol{v}\circ\boldsymbol{\pi}^i\sqrt{a}\circ\boldsymbol{\pi}^i\|\boldsymbol{\pi}^{i\prime}\|ds\\
&+\int_0^{\ell^i}\mathbf{q}^{j_1}\circ\boldsymbol{\pi}^i\boldsymbol{\nu}^{j_1}\circ\boldsymbol{\pi}^i\cdot\boldsymbol{w}\circ\boldsymbol{\pi}^i\sqrt{a}\circ\boldsymbol{\pi}^i\|\boldsymbol{\pi}^{i\prime}\|ds\\
&+\int_0^{\ell^i}\mathbf{p}^{j_2}\circ\boldsymbol{\pi}^i\boldsymbol{\nu}^{j_2}\circ\boldsymbol{\pi}^i\cdot\boldsymbol{v}\circ\boldsymbol{\pi}^i\sqrt{a}\circ\boldsymbol{\pi}^i\|\boldsymbol{\pi}^{i\prime}\|ds\\
&+\int_0^{\ell^i}\mathbf{q}^{j_2}\circ\boldsymbol{\pi}^i\boldsymbol{\nu}^{j_2}\circ\boldsymbol{\pi}^i\cdot\boldsymbol{w}\circ\boldsymbol{\pi}^i\sqrt{a}\circ\boldsymbol{\pi}^i\|\boldsymbol{\pi}^{i\prime}\|ds\\
&+\int_0^{\ell^i}\tilde{\boldsymbol{q}}^i\cdot(\boldsymbol{w}\circ\boldsymbol{\pi}^i)'ds+\int_0^{\ell^i}\tilde{\boldsymbol{p}}^i\cdot((\boldsymbol{v}\circ\boldsymbol{\pi}^i)'+\boldsymbol{t}^i\times\boldsymbol{w}\circ\boldsymbol{\pi}^i)ds=0,\quad(\boldsymbol{v},\boldsymbol{w})\in V_{\text{mixed}}.
\end{aligned}
$$

Thus, after integration by parts in the last two terms on the left hand-side, we obtain the differential form of the equations holding on all the edges:

$$
\begin{aligned}
&0=\tilde{\boldsymbol{p}}^{i\prime}-(\mathbf{p}^{j_1}\circ\boldsymbol{\pi}^i\boldsymbol{\nu}^{j_1}\circ\boldsymbol{\pi}^i+\mathbf{p}^{j_2}\circ\boldsymbol{\pi}^i\boldsymbol{\nu}^{j_2}\circ\boldsymbol{\pi}^i)\sqrt{a}\circ\boldsymbol{\pi}^i\|\boldsymbol{\pi}^{i\prime}\|,\\
&0=\tilde{\boldsymbol{q}}^{i\prime}+\boldsymbol{t}^i\times\tilde{\boldsymbol{p}}^i-(\mathbf{q}^{j_1}\circ\boldsymbol{\pi}^i\boldsymbol{\nu}^{j_1}\circ\boldsymbol{\pi}^i+\mathbf{q}^{j_2}\circ\boldsymbol{\pi}^i\boldsymbol{\nu}^{j_2}\circ\boldsymbol{\pi}^i)\sqrt{a}\circ\boldsymbol{\pi}^i\|\boldsymbol{\pi}^{i\prime}\|,\\
&\qquad i=1,\dots,n_E.
\end{aligned}
\tag{4.13}
$$

These equations determine the dynamic coupling conditions between the stent and Naghdi shell: the linear and angular momentum of the stent balance the normal components of the linear and angular momentum coming from the shell, acting on the reinforcing mesh. The terms coming from the action of the shell onto the stent play the role of the outside force $\tilde{\boldsymbol{f}}^i$ and angular moment $\tilde{\boldsymbol{g}}^i$ in equations (3.4) and (3.5).

Summary of the differential formulation for the coupled mesh-reinforced shell problem. We first present the summary of the differential formulation in terms of the shell and mesh sub-problems. The differential formulation of the coupled mesh-reinforced shell problem consists of the following:

Find $(\boldsymbol{u}, \boldsymbol{\omega}, \tilde{\boldsymbol{u}}, \tilde{\boldsymbol{\omega}})$ such that:

1) **The shell sub-problem.** Find the displacement $\boldsymbol{u}$ of the shell's middle surface, the infinitesimal rotation of its cross-sections $\boldsymbol{\omega}$, the force $\mathbf{p}$, and couple $\mathbf{q}$, such that the shell equations describing the balance of linear and angular momentum hold, with the corresponding constitutive laws, in the interior of each connected component ω^j, $j = 1, \dots, n_c$ bounded by stent struts, and the continuity of displacement boundary condition holding at the boundary of each connected component $\partial\omega^j$ bounded by the stent struts. This problem is further supplemented by the boundary conditions holding at the ends of the shell itself. More precisely, the problem is to find $(\boldsymbol{u}, \boldsymbol{\omega}, \mathbf{p}, \mathbf{q})$, such that in the interior of each ω^j, $j = 1, \dots, n_c$, the following holds:

$$\text{(4.14)} \qquad \left\{ \begin{array}{rcl} \operatorname{div}(\sqrt{a}\mathbf{p}) + \boldsymbol{f} & = & 0 \\ \operatorname{div}(\sqrt{a}\mathbf{q}) + \sqrt{a}\displaystyle\sum_{\alpha=1}^{2} \boldsymbol{a}_\alpha \times \mathbf{p}_\alpha & = & 0 \end{array} \right. \quad \text{in } \omega^j,$$

together with the constitutive relations:

$$\text{(4.15)} \qquad \begin{array}{rcl} \mathbf{p} & = & h\mathbf{Q}\mathcal{C}_m(\mathbf{Q}^T \left[\begin{array}{cc} \partial_1 \boldsymbol{u} + \boldsymbol{a}_1 \times \boldsymbol{\omega} & \partial_2 \boldsymbol{u} + \boldsymbol{a}_2 \times \boldsymbol{\omega} \end{array} \right]), \\ \mathbf{q} & = & \dfrac{h^3}{12}\mathbf{Q}\mathcal{C}_f\mathbf{Q}^T \nabla\boldsymbol{\omega}, \end{array}$$

and the boundary conditions on $\partial\omega^j$ given by the continuity of displacement between the shell and slender mesh rods reinforcing the shell:

$$\text{(4.16)} \qquad (\boldsymbol{u}, \boldsymbol{\omega}) = (\tilde{\boldsymbol{u}}, \tilde{\boldsymbol{\omega}}) \circ \boldsymbol{\pi}^{-1}, \quad \text{on} \quad \partial\omega^j, \quad j = 1, \dots, n_c.$$

Notice that problem (4.14), (4.15) is a differential problem for $(\boldsymbol{u}, \boldsymbol{\omega})$. The forces and couples can be recovered from (4.15) once $(\boldsymbol{u}, \boldsymbol{\omega})$ are calculated.

2) **The elastic mesh sub-problem.** Solve a large system of problems consisting of the static equilibrium problems for all the slender mesh components $e^i, i = 1, \dots, n_E$, which are coupled by the dynamic and kinematic coupling conditions holding at each vertex where the rods meet. More precisely, for each $i = 1, \dots, n_E$, find the displacements $\tilde{\boldsymbol{u}}^i$ from the middle line of the i-th rod, the infinitesimal rotation of the cross-sections $\tilde{\boldsymbol{\omega}}^i$, the forces and couples $\tilde{\boldsymbol{p}}^i$ and $\tilde{\boldsymbol{q}}^i$, such that in the interior of each slender rod the following equations, obtained from the mesh-shell dynamic coupling conditions (4.13), hold:

$$\text{(4.17)} \qquad \left\{ \begin{array}{rcl} \tilde{\boldsymbol{p}}^{i\prime} & = & [(\mathbf{p} \circ \boldsymbol{\pi}^i)(\boldsymbol{\nu}^i \circ \boldsymbol{\pi}^i)]\sqrt{a} \circ \boldsymbol{\pi}^i \|\boldsymbol{\pi}^{i\prime}\| \\ \tilde{\boldsymbol{q}}^{i\prime} + \boldsymbol{t}^i \times \tilde{\boldsymbol{p}}^i & = & [(\mathbf{q} \circ \boldsymbol{\pi}^i)(\boldsymbol{\nu}^i \circ \boldsymbol{\pi}^i)]\sqrt{a} \circ \boldsymbol{\pi}^i \|\boldsymbol{\pi}^{i\prime}\| \end{array} \right. \quad \text{on}$$
$$(0, \ell^i), \quad i = 1, \dots, n_E.$$

Here, the right hand-sides of equations (4.17) denote the jumps across the i-th rod e^i in the shell contact force $\mathbf{p}\circ\boldsymbol{\nu}^i$ and shell couple $\mathbf{q}\circ\boldsymbol{\nu}^i$. The normal $\boldsymbol{\nu}^i$, which lives in $\omega\subset\mathbb{R}^2$, is such that $\boldsymbol{\nu}^i$ and the vector determined by the parameterization of the i-th strut in ω, starting at the point associated with $s=0$, and ending at the point associated with $s=\ell^i$, form the right-hand basis. See Figure 4.

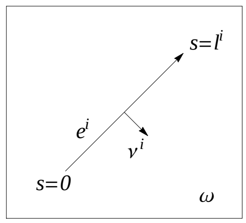

FIG. 4. *Normal ν^i to strut e^i in ω.*

Equations (4.17) are supplemented with the constitutive relations for each curved rod:

$$\tilde{\boldsymbol{q}}^i = \mathbf{Q}^i\mathbf{H}^i{\mathbf{Q}^i}^T\tilde{\boldsymbol{\omega}}^{i\prime}, \quad i=1,\dots,n_E, \tag{4.18}$$

and the inextensibility and unshearibility conditions:

$$0 = \tilde{\boldsymbol{u}}^{i\prime} + \boldsymbol{t}^i\times\tilde{\boldsymbol{\omega}}^i, \quad i=1,\dots,n_E. \tag{4.19}$$

The boundary conditions at $s=0,\ell^i$ for system (4.17)-(4.19) are given in terms of the coupling conditions that hold at mesh net's vertices $V\in\mathcal{V}$:

- The kinematic conditions describing continuity of displacement and infinitesimal rotation:

$$[\tilde{\boldsymbol{u}}]|_V = 0, \quad [\tilde{\boldsymbol{\omega}}]|_V = 0, \quad \forall V\in\mathcal{V} \tag{4.20}$$

- The dynamic conditions describing balance of forces and couples at each vertex $V\in\mathcal{V}$:

$$\sum_{i_V}(\pm1)\tilde{\boldsymbol{p}}^{i_V}|_V = 0, \quad \sum_{i_V}(\pm1)\tilde{\boldsymbol{q}}^{i_V}|_V = 0, \tag{4.21}$$

  where the sum goes over all the indices i_V corresponding to the edges meeting at the vertex V, and $\tilde{\boldsymbol{p}}^{i_V}|_V$ and $\tilde{\boldsymbol{q}}^{i_V}|_V$ denote the trace of $\tilde{\boldsymbol{p}}^{i_V}$ and $\tilde{\boldsymbol{q}}^{i_V}$ at V, respectively. The sign ±1 depends on the choice of parameterization of the i_V-th edge. The sign is positive for all the outgoing edges and negative for the incoming edges associated with vertex V. Solutions of the entire problem are independent of the choice of parameterization.

Equations (4.14)-(4.21) represent the differential formulation for the coupled mesh-shell problem. The shell and the reinforcing mesh are coupled via the kinematic coupling conditions, expressed in (4.16), describing continuity of displacement and infinitesimal rotation between the shell and slender mesh rods, and via the dynamic coupling conditions, expressed in (4.17), describing the balance of forces and couples between the shell and mesh. In the weak formulation, the kinematic coupling conditions are included in the solution space V_{coupled}, while the dynamic coupling conditions are imposed in the weak formulation (4.6).

The coupled shell-stent problem as a graph-based multi-component free-boundary problem defined on a collection of simply connected domains separated by graph's edges.

We can think of the coupled problem (4.14)-(4.21) as a free-boundary problem for the Naghdi shell $S = \boldsymbol{\varphi}(\bar{\omega})$, which is defined as a union of simply connected sub-shells $S^j = \boldsymbol{\varphi}(\omega^j)$, with the boundaries ∂S^j that are not known *a priori*, but are determined via an equilibrium problem for the position of stent struts. The position of stent struts, i.e., the stent's equilibrium, is influenced by the forces exerted by the shell onto the stent, and by the internal elastic energy associated with the elastic stent behavior. More precisely, the shell and stent are coupled through two sets of coupling conditions, the kinematic and dynamic coupling conditions. The kinematic coupling condition, describing no-slip between the shell and stent, plays the role of a Dirichlet boundary condition for each shell sub-problem defined on S^j. The dynamic coupling condition, describing the balance of contact forces and angular moments between the shell and stent, provides the additional information that is needed to determine the extra unknown in the problem, which is the position (and angular momentum) of the unknown boundary $\cup \partial S^j$.

This is a global problem, defined on an entire Naghdi shell S, whose solution depends not only on the elastic properties of the local shell and stent components, but also on the particular distribution of connected components S^j, which is determined by the geometry of the stent (graph).

5. Numerical examples. To illustrate the use of the coupled mesh-reinforced shell model we simulated four commercially available coronary stents on the US market, inserted in straight and bent arteries. The Naghdi shell model was used to simulate the mechanical properties of arterial walls, while the elastic mesh model discussed above was used to simulate the mechanical properties of coronary stents.

We discretized the coupled stent-reinforced artery model using a finite element method approach and implemented it within a publicly available software package FreeFem++ (see [19]). Triangular meshes were used in ω to approximate the Naghdi shell. Each mesh was aligned with the location of stent struts thereby discretizing the stent problem. No additional mesh was used for the 1D approximation of stent struts. P_2 elements (Lagrage quadratic polynomials) were used to approximate the Naghdi shell, thereby defining the P_2 elements for the stent model. They are accompanied by P_1 elements approximating the Lagrange multipliers associated with inextensibility of stent struts. The stiffness matrix for the stent was explicitly calculated and its values were then added to the corresponding elements of the stiffness matrix for the Nagdhi shell. For more details related to the mixed formulation and numerical approximation of the stent problem see [17].

Below we present several examples involving a cylindrical Naghdi shell simulating a virtual coronary artery, supported by four different types of stents available on the US market: a Palmaz-like stent, a Xience-like stent, a Cypher-like stent, and an Express-like stent. The Xience-like stent is assumed to be made of a cobalt-chromium alloy with $E = 2.43 \cdot 10^{11} Pa$, while the remaining stents are made of a 316L alloy of stainless steel with $E = 2.1 \cdot 10^{11} Pa$. The Poisson ratio is assumed to be $\nu = 0.31$. The struts' cross-sections are square, except for certain curly parts of the Cypher-like stent, which are rectangular with the thickness equal to 1/3 of the width. The lengths of the sides of the cross-sections are as follows:

	Palmaz-like	Xience-like	Cypher-like	Express-like
thickness/width	$10 \cdot 10^{-2} mm$	$8 \cdot 10^{-2} mm$	$14 \cdot 10^{-2} mm$	$13.2 \cdot 10^{-2} mm.$

The parameter values for the cylindrical Naghdi shell are the following: the reference diameter of the shell's middle surface is $2R = 3mm$ and length $33mm$. The shell is parametrized by

$$\boldsymbol{\varphi} : [-0.008, 0.025] \times [0, 2R\pi] \to \mathbb{R}^3, \qquad \boldsymbol{\varphi}(z,\theta) = (z, R\cos(\theta/R), R\sin(\theta/R)).$$

The thickness of the shell is $h = 0.58mm$, the Young modulus $E = 4 \cdot 10^5 Pa$ and the Poisson ratio $\nu = 0.4$.

In all the examples, an interior pressure of $10^4 N/mm^2$ was applied to the interior shell surface to inflate the shell and the response in terms of displacement and infinitesimal rotation was measured.

Two sets of boundary conditions are used:

- **Data 1.** The first set of boundary conditions simulates a straight coronary artery treated with a stent. The shell is assumed to be clamped, with zero displacement and zero rotation at the end points:

$$\boldsymbol{u} = (0,0,0), \quad \boldsymbol{\omega} = (0,0,0).$$

- **Data 2.** The second set of boundary conditions corresponds to a curved coronary artery treated with a stent. The shell is assumed to be clamped, with a given non-zero displacement and rotation at the end points of the shell prescribed in a way that causes bending of the shell:

$$\begin{array}{l} \boldsymbol{u} = (a_0 + \sin\alpha_0 R\cos(\theta/R), (\cos\alpha_0 - 1)R\cos(\theta/R), 0), \\ \boldsymbol{\omega} = (0,0,-\alpha_0), \end{array} \quad \text{at the left end,}$$

$$\begin{array}{l} \boldsymbol{u} = (-a_0 - \sin\alpha_0 R\cos(\theta/R), (\cos\alpha_0 - 1)R\cos(\theta/R), 0), \\ \boldsymbol{\omega} = (0,0,\alpha_0), \end{array} \quad \text{at the right end.}$$

Here $a_0 = L(1 - \sin\alpha_0/\alpha_0)/2$ is adjusted to reduce the stress of the elongation of the vessel. In the simulations we take the value $\alpha_0 = 15°$.

FIG. 5. *Vessel (shell) deformation without a stent, colored by radial displacement.*

5.1. Straight geometry with homogeneous boundary conditions. We begin by first considering a straight vessel without a stent, exposed to the internal pressure load of $10^4 N/mm^2$, and with homogeneous boundary conditions, as mentioned above in Data 1. Figure 5 shows that the pressure load inflates the vessel, as expected, with the maximum displacement of $4.21 \times 10^{-4} m$ taking place in the interior, away from the clamped end-points, giving rise to a boundary layer near the end points. This can be compared to the behavior of the same vessel but with a stent inserted in

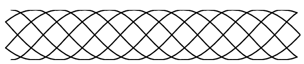

(a) Geometry of Palmaz-like stent

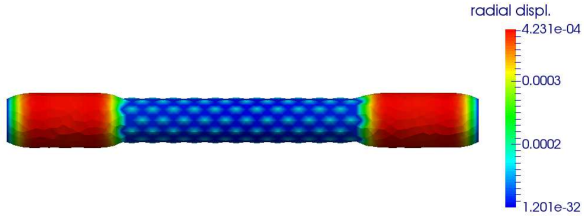

(b) Palmaz-like stent inserted in artery

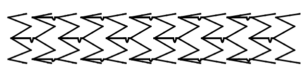

(c) Geometry of Xience-like stent

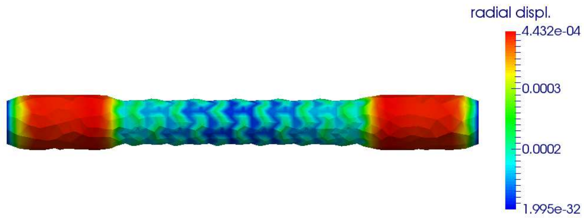

(d) Xience-like stent inserted in artery

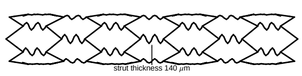

(e) Geometry of Cypher-like stent

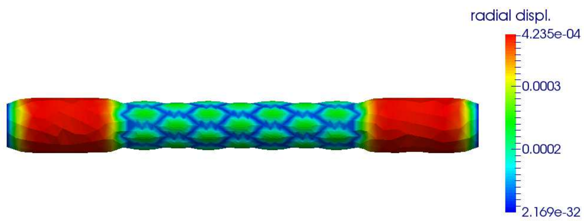

(f) Cypher-like stent inserted in artery

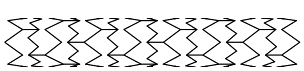

(g) Geometry of Express-like stent

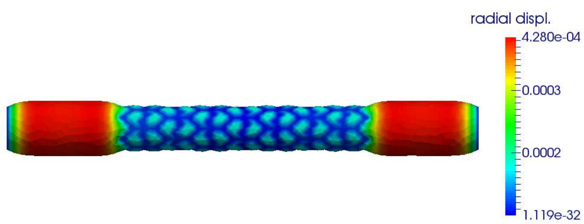

(h) Express-like stent inserted in artery

FIG. 6. *The figures of the left show the front view of the geometry of middle lines for each of the stents considered. The figures on the right show vessel deformation colored by radial displacement.*

it. In Figure 6 we show the deformation, colored by radial displacement, for the four stents inserted in the vessel. The same internal pressure loading onto the coupled stent-vessel configuration was considered with the pressure of $10^4 N/mm^2$ as before. Figure 6 shows that the effective properties of the vessel change with the stent insertion: the vessel-stent configuration is stiffer in the region where the stent is located, and less stiff away from the stent, giving rise to large displacement gradients near the end points of the stent. From the application point of view, the large strains near the

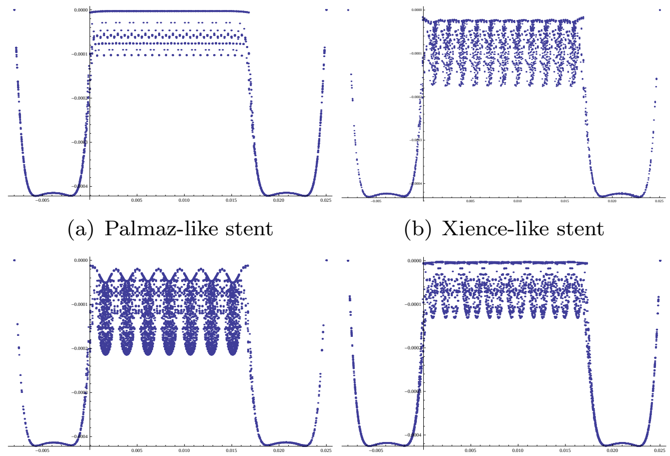

(a) Palmaz-like stent (b) Xience-like stent

(c) Cypher-like stent (d) Express-like stent

FIG. 7. *Radial displacement in terms of mesh points versus horizontal stent axis.*

proximal and distal end points of the stent may cause tissue damage and remodeling in arterial wall that may be a precursor for post-procedural complications associated with restenosis [25]. Our simulations shown in Figure 6 indicate that the most gradual change in displacement between the stented and non-stented region of the vessel occurs in the Xience-like stent considered in this numerical study. Figure 6 further shows that the geometry associated with the Palmaz-like stent and the Express-like stent considered in this study give rise to the stiffest stents when exposed to the internal pressure load in a straight vessel configuration. However, the result on Figure 6 show that all the stents when inserted into a vessel behave as stiff structures, allowing very small displacement at the location of stent struts.

A further inspection of the results shown in Figure 6 indicates vessel tissue protrusion in between the stent struts. A detailed view of radial displacement at all the mesh points is shown in Figure 7. In this figure we can see that the largest tissue protrusion in between the stent struts occurs for the Cypher-like stent, followed by the Xience-like stent, the Express-like stent, and the Palmaz-like stent. Again, the strains caused by tissue deformation in between the stent struts may be a precursor for in-stent restenosis, which remains to be an important clinical problem [1].

5.2. Curved geometry induced by non-homogeneous boundary conditions. We again begin by first considering a vessel without a stent, exposed to the internal pressure load of $10^4 N/mm^2$. In this example we take the boundary conditions causing bending, as described above in Data 2. Figure 8 shows that maximum radial displacement from the reference configuration, which is a straight cylinder, is at the "outer" surface of the cylinder, colored in red. Upon the insertion of a stent, the central region where the stent is located gets straightened out due to the increased stiffness of the coupled stent-shell configuration. Figure 9 shows deformation colored by radial displacement for the four stents considered in this work. The figures on the left show the reference (straight) stent configuration in grey and the superimposed deformed stent configuration, where the deformation is obtained with the boundary conditions specified in Data 2 above, with α_0 equal to one half of the α_0 used in the coupled stent-vessel configuration (each stent is half the length of the vessel). There-

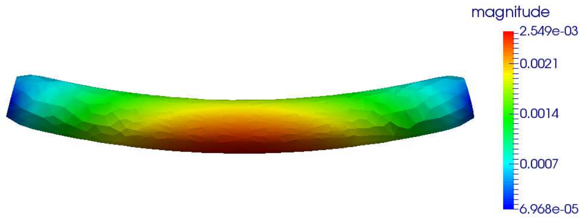

FIG. 8. *Vessel (shell) deformation without a stent, colored by radial displacement. Boundary conditions specified in Data 2 above, causing bending, were used.*

fore, the figures on the left show how the stent would bend without the presence of an artery, and the figures on the right show the coupled stent-vessel configuration resulting from the insertion of a stent into a bent vessel, where the bending of the vessel is caused by applying the boundary conditions from Data 2, above. Table 1 shows the radii of curvature for all the cases considered in Figure 9. We see that the stiffest stent to bending, when inserted into an artery, is the Palmaz-like stent, followed by the Cypher-like stent, the Express-like stent, and the Xience-like stent. The so called open-cell design of the Xience-like stent where every other horizontal stent strut is missing, makes this stent most pliable of all the stents considered in this study.

stent	radius of curvature stent	radius of curvature stent & vessel
no stent	-	0.061
Palmaz-like	0.0089	3.025
Xience-like	0.0085	0.854
Cypher-like	0.0089	2.697
Express-like	0.0088	1.166

TABLE 1

Radius of curvature of the stent with and without the vessel. The radius is calculated from three points, two at the ends and on in the middle of the stent.

We conclude this study by investigating the behavior of two Palmaz-like stents of half length inserted into a bent artery to see if this configuration would produce a more pliable solution to the treatment of the so called tortuous, i.e., curved arteries. Figure 10 shows the deformation colored by radial displacement of the coupled stent-vessel configuration. We calculated the radius of curvature and found out that for this two-Palmaz-like stent configuration the radius of curvature of the combined stent configuration is equal to 0.088, showing that this 2-stent configuration is even more pliable than the softest stent (Xience-like) considered in this study.

6. Conclusions. In this manuscript we presented a novel mathematical model which couples the mechanical behavior of a 2D Naghdi shell with the mechanical behavior of mesh-like structures, such as stents, whose 3D elastic behavior is approximated by a net/network of 1D curved rods. This is the first mathematical coupled model for mesh-reinforced shells involving reduced models. Each of the two reduced models has been mathematically justified to provide a good approximation of 3D elasticity when the thickness of the shell and the thickness of stent struts is small with respect to the larger dimension, which is the shell surface size or stent strut length [20, 21]. In the present manuscript we formulated the coupled model and proved the

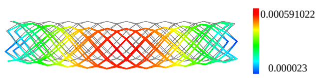

(a) Bent Palmaz-like stent

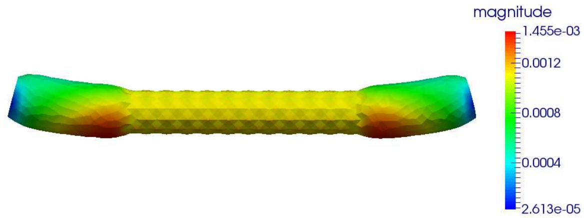

(b) Palmaz-like stent inserted in a bent artery

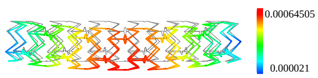

(c) Bent Xience-like stent

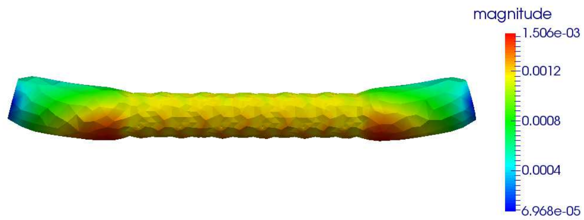

(d) Xience-like stent inserted in bent artery

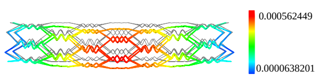

(e) Bent Cypher-like stent

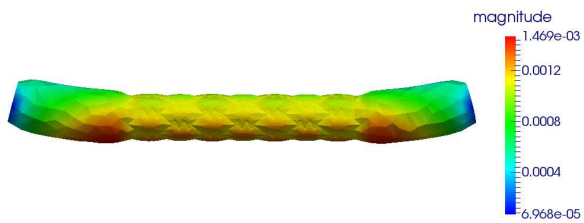

(f) Cypher-like stent inserted in bent artery

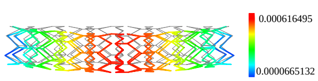

(g) Bent Express-like stent

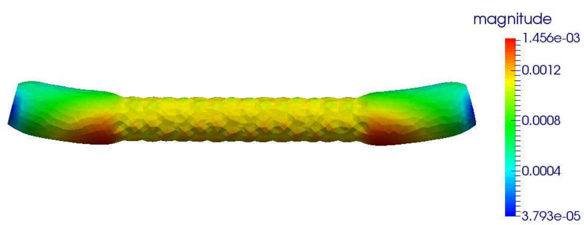

(h) Express-like stent inserted in bent artery

FIG. 9. *The figures on the left show the reference (in grey) and bent configuration (colored by radial displacement) for each of the four stents. The figures on the right show deformation of the vessel, colored by radial displacement, with a stent inserted into a bent vessel.*

existence of a unique weak solution to the proposed coupled shell-mesh problem by using variational methods and energy estimates.

The new Naghdi shell type model is particularly suitable for modeling the coupled shell-stent problem. It is given in terms of only two unknowns (the displacement of the middle surface, and infinitesimal rotation of cross-sections), it captures all three shell/membrane effects (stretching, transverse shear and flexion) allowing less regularity and the use of simpler Lagrange finite elements for the numerical simulation. The stent model, while it captures the full, leading 3D deformation of stent struts, it

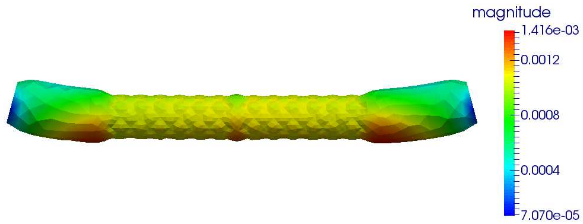

FIG. 10. *Deformation of the vessel with two Palmaz-like stents inside.*

has the computational complexity of 1D problems, allowing quick simulation of the coupled stent-vessel problem on a "standard" laptop computer such as, e.g., a 64-bit Windows 8.1 machine, with Intel i7 processor, and 16 GB RAM. When coupled with the shell problem, the size of the computational mesh for the coupled problem is *independent* of the thickness h of stent struts. This is never the case in 2D and 3D models capturing stent displacement, where the size of the computational mesh has to be much smaller than h, thereby giving rise to large memory requirement and high computational costs.

Several numerical examples of coronary stents were presented. Each coupled stent-vessel simulation used a mesh of 1500-3000 nodes. Stents with more complex geometries, such as the sinusoidal struts in the Cypher-like stent, require higher resolution, involving 3000 nodes. The simulations take between 5 and 10 minutes on a 64-bit Windows 8.1 machine, with Intel i7 processor, and 16 GB RAM. The simple implementation, low computational costs, and low memory requirements make this model particularly suitable for fast algorithm design, which can be easily coupled with a fluid sub-problem leading to an efficient, accurate, and computationally feasible fluid-structure interaction algorithm simulating the behavior of e.g., vascular stents interacting with blood flow and vascular wall. Using this model in a fluid-structure interaction (FSI) algorithm modeling the interaction between blood flow and vascular stents inserted in a vascular wall would be an improvement over the FSI approaches in which the presence of a stent is modeled by modifying the elasticity coefficients in the elastic wall, see, e.g., [4]. The model proposed in the current work would provide a true fluid-composite structure interaction algorithm in which the stent and the vessel are modeled as a fully coupled mesh-reinforced shell.

REFERENCES

[1] F. Alfonso, R.A. Byrne, F. Rivero, A. Kastrati. Current Treatment of In-Stent Restenosis. *J Am Coll Cardiol.* 63(24), 2659–2673, 2014.

[2] S. S. Antman. Nonlinear Problems of Elasticity. Springer, New York, 2005.

[3] J. L. Berry, A. Santamarina, J. E. Moore Jr., S. Roychowdhury and W. D. Routh. Experimental and Computational Flow Evaluation of Coronary Stents. *Annal of Biomedical Engineering*, 28, 386–398, 2000.

[4] M. Bukač, S. Čanić, B. Muha. A Nonlinear Fluid-Structure Interaction Problem in Compliant Arteries Treated with Vascular Stents *Applied Mathematics and Optimization* 73(3), pp. 433-473, 2016.

[5] M. Bukac, S. Canic, R. Glowinski, J. Tambaca, A. Quaini. Fluid-structure interaction in blood flow capturing non-zero longitudinal structure displacement. *Journal of Computational Physics* 235, 515-541, 2013.

[6] M. Bukac and S. Canic. Longitudinal displacement in viscoelastic arteries: a novel fluid-structure interaction computational model, and experimental validation. *Journal Mathematical Biosciences and Engineering*10(2), 258-388, 2013.

[7] J. Butany, K. Carmichael, S.W. Leong, M.J. Collins. Coronary artery stents: identification and evaluation. Review. *J Clinical Path* 58, pp. 795-804, 2005.
[8] S. Čanić, J. Tambača, Cardiovascular Stents as PDE Nets: 1D vs. 3D, *IMA Journal of Applied Mathematics* 77 (6), 748–779, 2012.
[9] S. Canic, J. Tambaca, G. Guidoboni, A. Mikelic, C.J. Hartley, D. Rosenstrauch. Modeling viscoelastic behavior of arterial walls and their interaction with pulsatile blood flow. *SIAM J Applied Mathematics* 67(1) 164-193, 2006.
[10] D. Q. Cao, R. W. Tucker. Nonlinear dynamics of elastic rods using the Cosserat theory: Modelling and simulation, *International Journal of Solids and Structures* 45 (2), pp. 460-477, 2008.
[11] Ciarlet, Philippe G. Mathematical elasticity. Vol. I. Three-dimensional elasticity, North-Holland Publishing Co., Amsterdam, 1988.
[12] P.G. Ciarlet, Mathematical elasticity. Vol. III. Theory of shells. Studies in Mathematics and its Applications, 29. North-Holland Publishing Co., Amsterdam, 2000.
[13] C. Dumoulin and B. Cochelin. Mechanical behaviour modelling of balloon-expandable stents. *Journal of Biomechanics,* 33 (11), 1461–1470, 2000.
[14] A. O. Frank, P. W. Walsh and J. E. Moore Jr.. Computational Fluid Dynamics and Stent Design. *Artificial Organs* 26 (7), 614–621, 2002.
[15] C.A. Figueroa, I.E. Vignon-Clementel, K.E. Jansen, T.J.R. Hughes, C.A. Taylor. A coupled momentum method for modeling blood flow in three dimensional deformable arteries, *Comp. Meth. Appl. Mech. Eng.*, 195(41-43), 5685-5706, 2006.
[16] G. Griso. Asymptotic behavior of structures made of curved rods. *Anal. Appl.* (Singap.) 6 (1), 11–22, 2008.
[17] L. Grubišić, J. Iveković and J. Tambača, Numerical approximation of the equilibrium problem for elastic stents. In preparation (2016).
[18] V. Hoang. Stent Design and Engineered Coating Over Flow Removal Tool, Team #3 (Vimage), 10/29/04.
[19] FreeFem++ *Université Pierre et Marie Curie, Laboratoire Jacques-Louis Lions.* `http://www.freefem.org/`
[20] M. Jurak and J. Tambača, Derivation and justification of a curved rod model, *Mathematical Models and Methods in Applied Sciences*, 9 (1999) 7, pp. 991–1014.
[21] M. Jurak and J. Tambača, Linear curved rod model. General curve, *Mathematical Models and Methods in Applied Sciences*, 11 (2001) 7, pp. 1237–1252.
[22] D. R. McClean and N. Eigler. Stent Design: Implications for Restenosis. *MedReviews*, LLC, 2002.
[23] F. Migliavacca, L. Petrini, M. Colombo, F. Auricchio and R. Pietrabissa. Mechanical behavior of coronary stents investigated through the finite element method. *Jurnal of Biomechanics* 35 (6), 803–811, 2002.
[24] J. E. Moore Jr. and J. L. Berry. Fluid and Solid Mechanical Implications of Vascular Stenting. *Annals of Biomedical Engineering* 30 (4), 498–508, 2002.
[25] A. C. Morton, D. Crossman and J. Gunn. The influence of physical stent parameters upon restenosis. *Pathologie Biologie*, 52 (4), 196–205, 2004.
[26] P.M. Naghdi, The theory of shells and plates, Handbuch der Physik, vol. VIa/2, Springer-Verlag, New York, 1972, pp. 425-640.
[27] F. Nobile, C. Vergara. An effective fuid-structure interaction formulation for vascular dynamics by generalized Robin conditions, *SIAM J Sci Comp* 30(2), 731-763, 2008.
[28] L. Scardia. The nonlinear bending-torsion theory for curved rods as Γ-limit of three-dimensional elasticity. *Asymptot. Anal.* 47: 317-343, 2006.
[29] J. Tambača, A note on the "flexural" shell model for shells with little regularity, *Advances in Mathematical Sciences and Applications* **16** (2006), 45–55.
[30] J. Tambača, A model of irregular curved rods, in: Applied mathematics and scientific computing (Dubrovnik, 2001). Kluwer/Plenum: New York, 2003, 289–299.
[31] J. Tambača, *A new linear shell model for shells with little regularity*, Journal of Elasticity **117** (2014), 2, 163-188.
[32] J. Tambača, M. Kosor, S. Čanić, D. Paniagua, Mathematical modeling of vascular stents, *SIAM J. Appl. Math.* 70 (2010), no. 6, 1922–1952.
[33] J. Tambača and Z. Tutek, A new linear Naghdi type shell model for shells with little regularity. Applied Mathematical Modelling. 40(23-24) 10549-10562, 2016.
[34] L. H. Timmins, M. R. Moreno, C. A. Meyer, J. C. Criscione, A. Rachev and J. E. Moore Jr.. Stented artery biomechanics and device design optimization. *Med. Bio. Eng. Comput* 45 (5), 505–513, 2007.